Doctoral Dissertation

Coherent choice-direction representations between task epochs are supported by dynamic coordination of the perirhinal cortical neurons

Tomoya Ohnuki

Graduate School of Brain Science, Doshisha University

May. 2020

Abstract

Cortical neurons show distinct firing patterns across multiple epochs of a given task, such as cue, action, and reward, which are characterized by different computational aspects. Recent computational approaches suggest that such distinct response patterns underlay dynamic population-level structures supporting computational flexibility served by a neural population. On the other hand, individual neurons in some cortical areas often show coherent response patterns across different task-epochs, suggesting their ability to form higher-order representations by integrating relevant information. Because of the difference in the explanations in these studies (that is, population or single-neuron level), it is still elusive how such coherent single-neuron representations are reconciled with the dynamically changing population-level structure. To synthesize our understanding of these apparently different hypotheses, I analyzed neural responses in the perirhinal cortex (PRC) where robust neural responses in various task-epochs have been reported, with a focus on the cue and reward epochs of a standard two-alternative forced-choice task. I found that the PRC neurons often

encoded choice-direction (left/right) information during the task and substantially inverted such selectivity between the cue and reward epochs, suggesting a form of coherent single-neuron representation in the PRC. When the rats erroneously performed the task, the choice-direction encodings were decreased in the reward epoch but not in the cue epoch. The distinct effects of erroneous performance indicated different neural computations carried out in these task-epochs. By using the principal component analysis, I identified two-dimensional neural subspaces associated with each of the epochs, which summarized the population response of the PRC as the weighted sum of individual neural responses. The cue and reward epochs shared the first neural dimensions where the choice directions were consistently discriminated. Interestingly, those dimensions were supported by only moderately correlated weighting patterns across the neurons, and the individual neurons dynamically changed their contributions to the entire population between the epochs. These results suggest heterogeneous computational roles of individual neurons that hold temporally coherent representations.

Acknowledgments

I would like to express my deepest gratitude to my supervisors, Dr. Yoshio Sakurai and Dr. Junya Hirokawa for their continuous guidance, scientific advice, and encouragement during the last 5 years. I also thank Dr. Hiroyuki Manabe and the past and present lab members for their encouragement and insightful comments on this research.

I would like to give special thanks to my thesis committee, Dr. Susumu Takahashi, Dr. Shigeo Takamori, and Dr. Takeshi Sakaba for their time and efforts in my examination.

I am also grateful to the Japan Society for the Promotion of Science (JSPS) and Doshisha University for their financial support.

Finally, I wish to extend my sincere gratitude to my family for their understanding, support, and encouragement. I believe I could not have achieved this study without their dedication.

Table of contents

List of figures and tables

Chapter 1. Introduction

1.1. Two major hypotheses for functional flexibility of cortical neurons

1.1.1. Flexible responses of individual cortical neurons to multiple task-epochs

Neural representations in cortical areas have long been investigated by analyzing neural responses in specific epochs of a given behavioral task, which correspond to hypothesized functional features of the area of interest. For instance, neurons in the visual cortices have been studied by analyzing their responses during the presentation of cue stimuli in visual tasks, and abundant visual representations in those areas have been revealed (Bruce, et al., 1981; Hubel & Wiesel, 1959). However, it is known that even neurons in the primary visual cortex carry not only cue information but also others such as reward-anticipation signals in the absence of sensory inputs (Shuler & Bear, 2006). In particular, in higher-order cortical areas where diverse inputs converge, it is well-known that individual neurons show flexible response to multiple task-epochs characterized by apparently different computational demands, such as cue, action, and reward (**Fig. 1**; Sakurai, et al, 2017;

Sakurai, 1990a; 1990b). These observations suggest that such functional flexibility is one of the intrinsic features of cortical neurons.

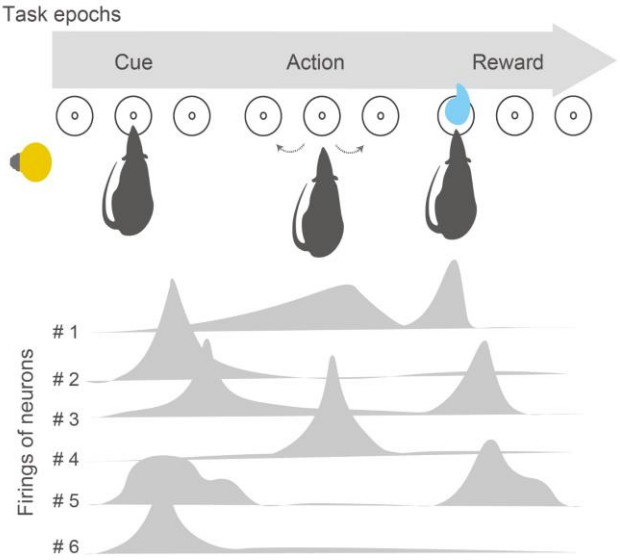

Figure 1 | Flexible responses of individual neurons to multiple epochs of a given task.

Schematic drawing of the animal performing a two-alternative choice task (upper), in which three task-epochs with different computational demands: cue, action (for choice), and reward. When responses of neurons from a given higher-order cortical are recorded during the task performance, neurons that modulate their firing rates in various task-epochs can be detected (bottom).

1.1.2. Population-level hypothesis

Recent computational approaches have shown that such flexible single-neuron responses are only interpretable in terms of their contributions to dynamic population-level structures, which realize distinct computations in different task-epochs (Lara et al., 2018; Parthasarathy et al., 2017; Mendoza-Halliday & Martinez-Trujillo, 2017; Elsayed et al., 2016; Raposo et al., 2014; Mante et al., 2013). In the view of population-level structures, individual neurons are considered to encode only a fraction of information completed by the entire population, and thus they frequently encode combinations of irrelevant information that cannot be interpreted as explicit representations at single-neuron levels. The studies based on this view often highlight the complex changes occurring in responses of a neural population between different task-epochs, which can provide orthogonal neural subspaces (that is, subspaces defined by a linear combination of the firings of all neurons in a population; **Fig. 2**). When population response patterns randomly change between two task-epochs, neural subspaces associated with these epochs become orthogonal and can carry out independent computations. The orthogonal subspaces are regarded as a population-level mechanism to

control what signals in a given population are transmitted to what downstream areas during different epochs (Raposo et al., 2014).

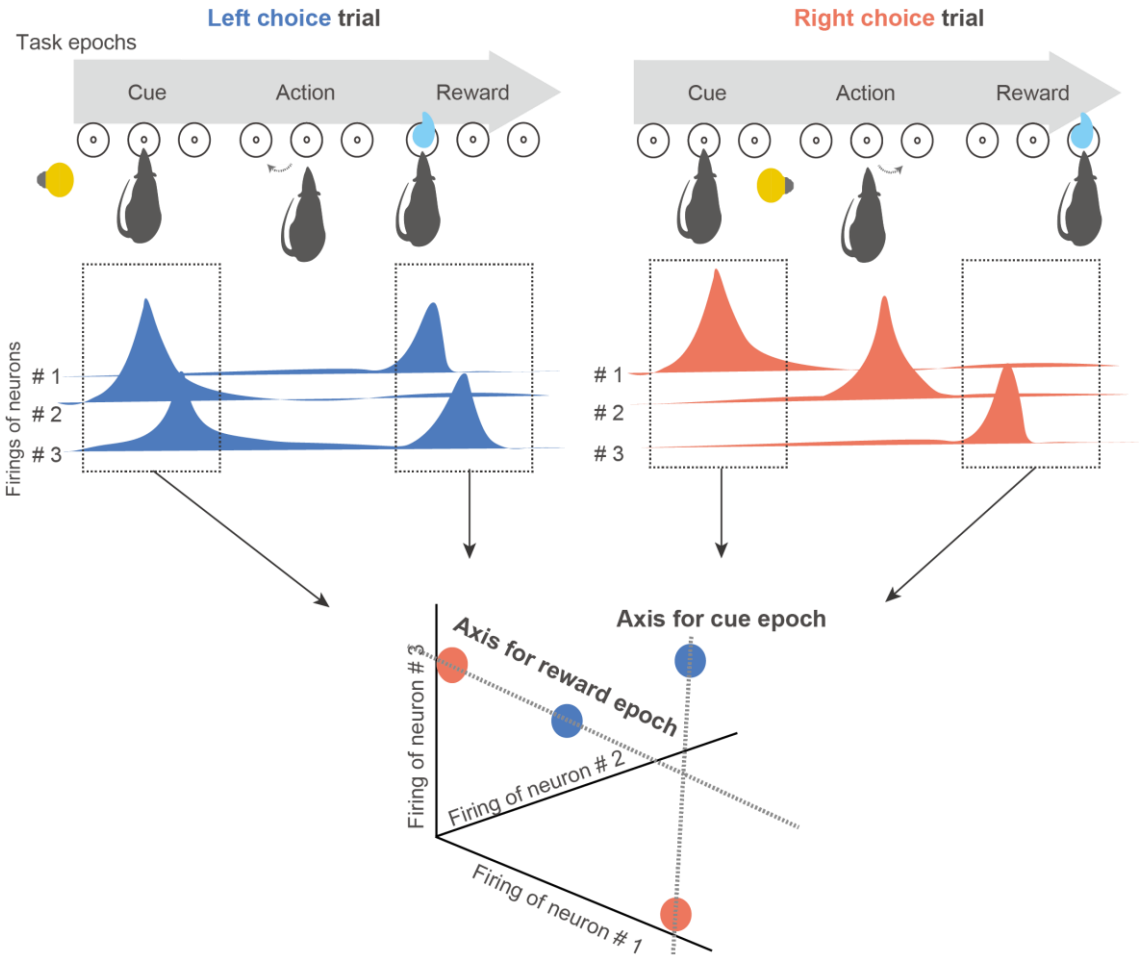

Figure 2 | Dynamic population encoding supporting independent computations between multiple task-epochs.

Schematic drawing of the animal performing a two-alternative choice task with three different task-epochs (upper). The left choice trial and right choice trial are independently depicted. For simplicity, I here consider the responses of a neural population composed of three neurons in the cue and reward epochs. The responses of the neurons are shown for each trial type (middle; blue, left trial; red right trial). In the left trial, the neurons 2 and 3 modulate their firings in the cue epoch (shown by the first rectangle in the left). On the other hand, in the reward epoch, the neurons 1 and 3 modulate their firings. Also, in the right trial, the neuron 1 responds during the cue epoch, but the neuron 3 responds in the reward epoch. As shown in the bottom, the time-averaged response of the population during each epoch can be represented as a point in a subspace defined by the firings of the individual neurons. In this case, as shown by the dashed lines, the choice information in the cue and reward epochs are captured by the nearly orthogonal axes. In other words, the neural response patterns are independent between the epochs at the population-level.

1.1.3. Single-neuron level hypothesis

In contrast, traditional single-neuron level approaches have shown that individual neurons in many cortical areas often encode relevant information across multiple task-epochs (Hirokawa et al., 2019; Guo et al., 2017; Eradath et al., 2015; Gardner & Fontanini, 2014; Kennerley & Wallis, 2009; Furuyashiki et al., 2008; Hosokawa et al., 2005). Such coherent single-neuron responses suggest their individual ability to support relevantly integrated representations through different task-epochs (**Fig. 3**). For instance, a subset of neurons in the anterior cingulate cortex coherently encodes predicted and experienced reward and thus is considered to form integrated value representations (Kennerley & Wallis, 2009). This approach has successfully identified the typical functions of each higher-order cortical area.

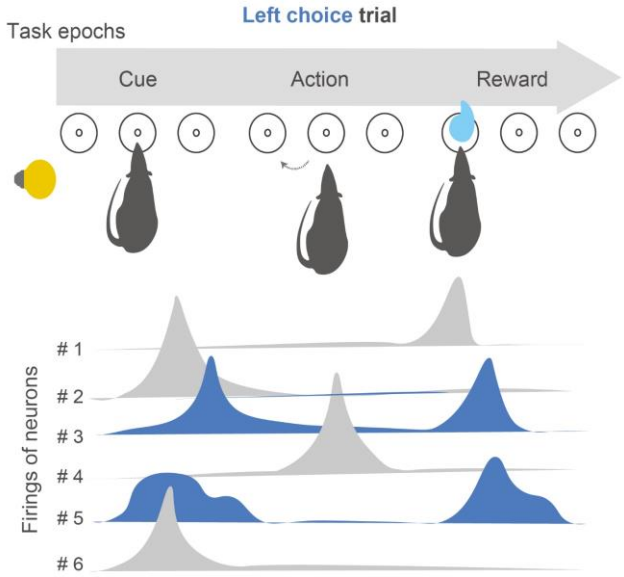

Figure 3 | Coherent single-neuron encodings between different task-epochs.
Schematic drawing of the animal performing a two-alternative choice task with three different task-epochs (upper). For simplicity, only the left trial is depicted here (bottom). The neuron 3 and 5 modulate their firings in both cue and reward epochs and convey the left choice information across the explicitly different epochs. In the traditional single-neuron level view, such neurons with temporally coherent responses are regarded as a form of coherent neural representation integrated across task epochs with distinct computations.

1.1.4. Relationships between population-level and single-neuron-level approaches

Because of the differences in the forms of explanation in these studies (that is, population or single-neuron level), how coherent representations carried by individual neurons can be reconciled with dynamically changing population structure has not been well investigated. One possible solution is to combine both scales of analysis in a single study and directly examine how neurons with temporally coherent responses work under the dynamics of the entire neural population. To implement such a study, I focused on a higher-order cortical area, the perirhinal cortex (PRC), which resides in the medial temporal lobe. In the following section, I shortly describe the anatomical and functional features of this cortical area.

1.2. The perirhinal cortex as a higher-order cortical area

The PRC receives sensory inputs from almost all the modalities from the primary and secondary sensory cortices, reward-related signals from the amygdala, and contextual information from the prefrontal cortex, entorhinal cortex, and hippocampus (Tomas Pereira et al., 2016; Furtak et al., 2007; Burwell, 2001). The diverse inputs evoke robust neural responses in multiple task-epochs in the PRC (Eradath et al., 2015; Ohyama et al., 2012). A well-known function of the PRC is recognition memory, which is supported by coherent single-neuron responses to the target identity (for example, a specific object regardless of its size, view angle, and color). The coherence of single-neuron responses is observed across explicitly different task-epochs such as cue and reward, suggesting that the PRC neurons encode associative memory for targeted information (for example, a specific stimulus or choice in conjunction with reward) (Eradath et al., 2015). On the other hand, it has also been shown that individual neurons in the PRC flexibly encode visual stimuli during the cue presentation and choice during movements for choices (Ahn & Lee, 2017). These results suggest the capacity of the PRC neural population to employ both population-level dynamics and coherent

representations through multiple task-epochs.

1.3. Investigating population dynamics and coherent single-neuron responses in the PRC

To investigate how the PRC shows coherent single-neuron representations and population dynamics across different task-epochs, I employed a standard two-alternative forced-choice task and focused on neural responses in two epochs, where different computations are demanded: making predictions about the outcome of choices (cue epoch) and reinforcing the choices (reward epoch). By taking advantage of the interleaved visual and olfactory cue stimuli, which allowed us to evaluate modality-independent encodings, I analyzed dynamic population encodings related to different choices during those epochs in relation to single-neuron level encodings.

Chapter 2. Materials and Methods

2.1. Subjects

Seven male Long-Evans rats (Shimizu Laboratory Supplies, Kyoto, Japan) weighting 278–375 g at the beginning of the training were individually housed and maintained on a laboratory light/dark cycle (lights on 8:00 A.M. to 9:00 P.M.). Rats were placed on water restriction with *ad libitum* access to food. The animals were maintained at 80% of their baseline weight throughout the experiments. All experiments were implemented in accordance with the guidelines for the care and use of laboratory animals provided by the Animal Research Committee of the Doshisha University with its approval.

2.2. Behavioral task

2.2.1. Apparatus

An operant chamber (O'Hara, Tokyo, Japan) with three ports in the front wall for nose-poke responses was enclosed in a soundproof box (Brain Science Idea, Osaka, Japan). Each port was equipped with an infrared sensor to detect the animals' nose-poke responses. Visual cues were presented using white light-emitting diodes (LEDs) (4000 mcd; RS Components, Yokohama, Japan) placed on the left and right walls of the operant chamber, as in **Fig. 8a**. Cue odors were presented via the central port through a stainless tube. The odors were mixed with pure air to produce a 1:10 dilution at a flow rate of 60 ml/min using a custom-built olfactometer (AALBORG, Orangeburg, NY). Water rewards were delivered from gravity-fed reservoirs regulated by solenoid valves (The Lee Company, Westbrook, CT) through stainless tubes placed inside of the left and right target-ports. Stimulus and reward deliveries and measurements of behavioral responses were performed by using Bpod and Pulse Pal (**Fig. 4**; Sanders & Kepecs, 2014; Sanworks, Stony Brook, NY).

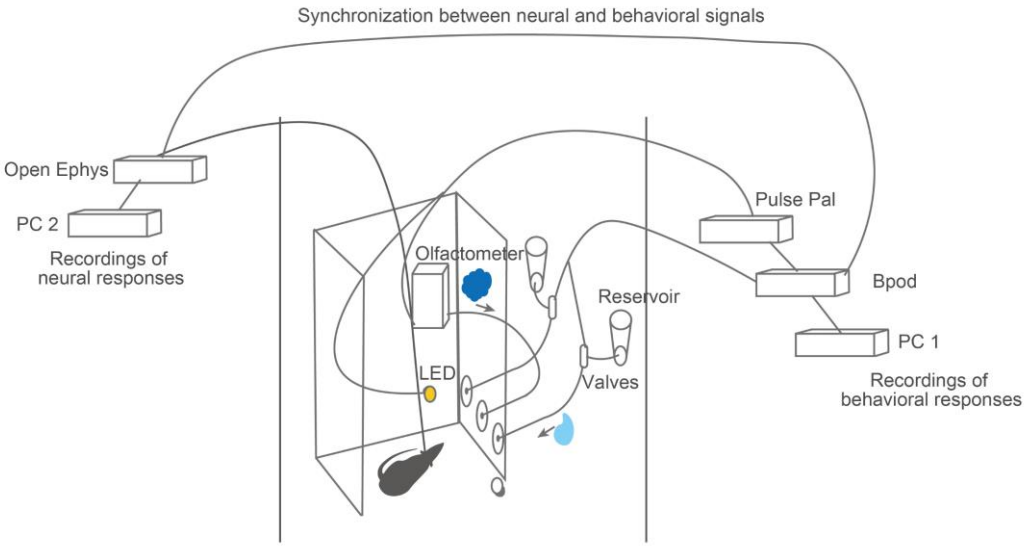

Figure 4 | Schematic drawing of the apparatus for the behavioral task.

2.2.2. Two-alternative forced-choice task

Each trial started when the rats poked their snout into the central port (**Fig. 8b**). After a variable delay (200–600ms, uniform distribution), a cue randomly selected from four stimuli (left/right LED for visual modality, S(+)/R(–)-2-octanol for olfactory modality) was delivered. If the rats successfully maintained their nose in the central port during 1 s after the cue onset, the "go" sound was delivered, and they were allowed to withdraw from the central port and to choose either left or right target port based on the task rule (bottom right in **Fig. 8a**). The presentations of the cue and the go sound were terminated by the withdrawal from the central port. When the rats left the central port without waiting for the go sound, the trial was canceled and followed by a 5 s punish intertrial-interval. Only correct choices were immediately rewarded by a drop of water (13 μl for five rats and 16 μl for two rats), from the target port. Rats performed 861 ± 232 trials in a daily recording session (seven rats, 50 sessions).

For two of seven rats (**Fig. 11**), a 500 ms delay period was inserted between the onset of the target choice and the reward to assess the potential influence of non-orienting movements (licking) and spatial view on neural

responses.

2.2.3. Training

I trained the rats step-by-step to perform the task described above. The training period typically lasted 4 to 8 weeks. First, rats were trained to poke into the central port and then collect the water reward (20 μl) from the left or right target-port. The duration of the central poke was gradually extended by delaying the go sound up to 1 s after the poke onset. Next, the rats were trained to discriminate the odor cues based on the same contingencies as the recording sessions. A variable delay (200–600 ms) was inserted before the cue onset. After the rats became able to successfully discriminate the odor cues (> 80%), they were also trained to discriminate the visual cues based on the same contingencies as the recording sessions (> 80%). Finally, visual and olfactory trials were interleaved within a session, and the animals were trained to perform the task according to a training performance criterion (> 80%).

For the two rats (**Fig. 11**), a reward delay period was introduced after they acquired the odor discrimination. The reward delay was gradually extended from 100 to 500 ms.

2.2.4. Mixture of odors

The cue odors, S(+)/R(–)-2-octanol, were mixed together in a subset of sessions in order to increase the difficulty of the olfactory discrimination and thereby obtaining a sufficient number of erroneous trials. For instance, I used a 60/40 ratio in a given session, delivering an odor mixture of 60% S(+)-2-octanol and 40% R(–)-2-octanol. The odor discrimination accuracy was kept constant (> 80%) throughout the recording sessions by adjusting the degree of odor mixing before each session.

2.3. Surgery

Rats were anesthetized with 2.5% isoflurane before surgery, and it was maintained throughout surgical procedures. I monitored body temperature, movements, and hind leg reflex and adjusted the depth of the anesthesia as needed. An eye ointment was used to keep the eyes moistened throughout the surgery. Subcutaneous scalp injection of a lidocaine 1% solution provided local anesthesia before the incision. The left temporalis muscle was retracted to expose the skull during the surgery. A craniotomy was performed over the anterior part of the left PRC (AP −3.5 to −3.24 mm, ML 6.6 to 6.8 mm relative to the bregma, 3.5 to 4.0 mm below the brain surface) and a custom-designed electrode was vertically implanted using a stereotactic manipulator. A stainless-steel screw was placed over the cerebellum and served as the ground during the recordings. The mean response of all electrodes was used as a reference. During a week of postsurgical recovery, the tetrodes were gradually lowered to detect unit activities in the PRC. Electrode placement was estimated based on the depth and was histologically confirmed at the end of the experiments.

2.4. Electrophysiological recordings

2.4.1. Electrodes for extracellular recordings

A custom-designed electrode composed of eight tetrodes (tungsten wire, 12.5 μm, California Fine Wire, Grover Beach, CA) was used for the extracellular recordings. The tetrodes individually covered by a polyimide tube (A-M Systems, Sequim, WA) were placed at a 100 μm separation, and typically had an impedance of 150–700 kΩ at 1 kHz. The signals were recorded with Open Ephys (Cambridge, MA) at a sampling rate of 30 kHz and bandpass filtered between 0.6 and 6 kHz. The tetrodes were lowered approximately 80 μm after each recording session, and thereby independent populations of neurons were recorded across the sessions.

2.4.2. Spike sorting and screening criteria of units

All analyses were performed using MATLAB (MathWorks, Natick, MA). To isolate single-neuron responses from the recorded neural data, the spikes were manually clustered with MClust (A.D. Redish) for MATLAB (**Fig. 5**). Only neurons met the following criteria were included for further analyses: (1) units with sufficient isolation quality (isolation distance ≧ 15); (2) units with reliable refractory periods (violations were less than 1% of all spikes); and (3) units with sufficient mean firing rates in the 1 s after the cue onset (> 0.5 Hz). On average, 10.9 ± 7.4 neurons were detected in a single recording session, and 6.2 ± 3.4 neurons survived these quality criteria (total of 312 neurons from seven rats).

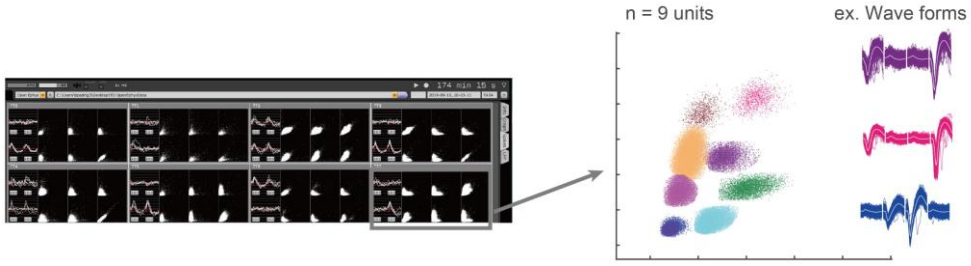

Figure 5 | Clustering of single-neuron responses from the recorded data.
The left panel shows the recording history display of a recording session. The right panel shows the detected nine single-neurons from a tetrode. The clusters in different colors indicate different single-neurons. The lines shown in the right indicate the spike waveforms of three example neurons. The colors correspond to those of the clusters.

2.4.3. Histology

Once the experiments were completed (**Fig. 6**), the rats were deeply anesthetized with sodium pentobarbital and then transcardially perfused with phosphate-buffered saline and 4% paraformaldehyde. The brains were removed and post-fixed in 4% paraformaldehyde, and 100 μm coronal sections of the brains were prepared to confirm the recording sites (**Fig. 9**).

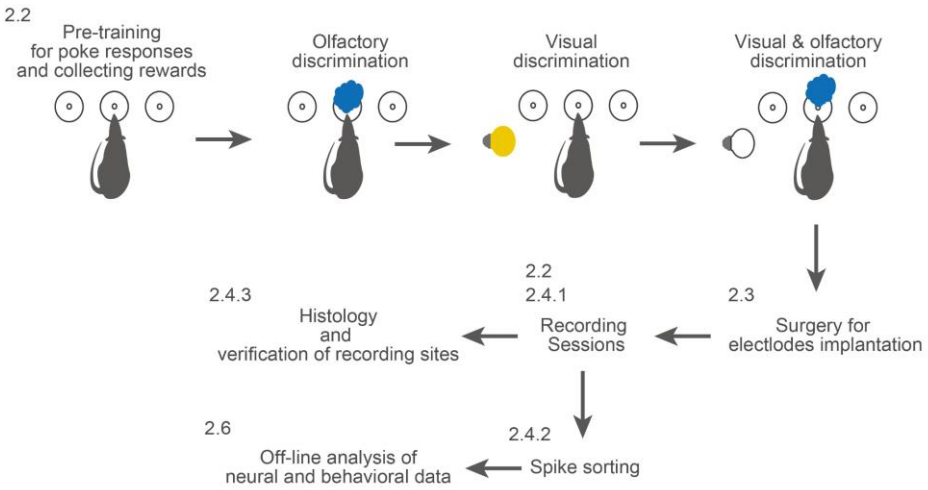

Figure 6 | A flow chart representing the procedure of the experiments and analyses in this study.
The numbers shown in this figure correspond to the number of chapters including each procedure.

2.5. Monitoring and processing of body posture during task performance

I used a head-mounted accelerometer (Intan Technologies, Los Angeles, CA) to obtain postural signals from the animals (n = 2) during the electrophysiological recordings (**Fig. 11**). The accelerometer signals (x-, y-, z-axis) were recorded at a sampling rate of 30 kHz and then downsampled to 100 Hz. To precisely detect the body posture of the animals, gravity components of the accelerometer signals were estimated by using a low-pass filter with a cut-off frequency of 2 Hz (Meyer et al., 2018). To reduce the influence from the head angle that each animal typically preferred (Meyer et al., 2018), for each axis, the above-processed signals were normalized to the mean and standard deviation in the baseline epoch (−400 to 0 ms before the cue onset).

2.6. Analysis

2.6.1. Selective responses to different choice directions

In order to evaluate the selective responses to different directions of choices, choice-direction selectivity (Hirokawa et al, 2011) was computed. I first grouped correct trials into four types based on the cue modality (visual or olfactory) and target choice (left or right). For each modality, I independently calculated the choice-direction selectivity by using ROC analysis (Green & Swets, 1966). The choice-direction selectivity was obtained from the area under the ROC curve (AUC) and defined as $2 \times (\mathrm{AUC} - 0.5)$ ranging from -1 to 1. In this analysis, a positive value indicated a neuron selectively fired to the left target-choice, and a negative value indicated the opposite. A value of zero indicated the absence of choice-direction selective responses. To determine statistical significance ($P < 0.05$), I used permutation tests (1,000 iterations). For visualization of the temporal patterns of the choice-direction selectivity in individual neurons (**Fig. 10–12**), the mean firing rates were computed in 10 ms time windows (smoothed with a Gaussian, $\sigma = 30$ ms), and I then computed the choice-direction selectivity at each time point from those data.

2.6.2. Statistics

The statistical significance of the decoding analysis and the state-space analysis was evaluated with a bootstrapping procedure (Parthasarathy et al., 2017). I estimated the P value for the bootstrapping procedure by computing the ratio $(1+X) / (N+1)$, where the number X indicates overlapping data points between the two distributions, and the number N indicates iterations. Since I used 1,000 bootstraps, two distributions with no overlap resulted in $P < 0.001$, and two distributions with x% overlap resulted in $P \approx x/100$.

All the data are presented as mean ± standard deviation unless otherwise stated. Individual statistical tests are described where referenced in the manuscript.

2.6.3. Decoding analysis

A cross-temporal pattern analysis (Spaak et al., 2017; Stokes et al., 2013) was employed to investigate the temporal changes in the choice-direction selective responses in the PRC. Neural responses were pooled across the recording sessions to maximize the number of neural responses included in the decoding analysis. Here, I refer to the pooled pseudo-population of the PRC neurons (n = 207 from five rats) as the full population. The instantaneous firing rate of each neuron was estimated by the spike counts in a 150 ms sliding window (10 ms increment). I computed the above described choice-direction selectivity from the instantaneous firing rates for each neuron independently for visual and olfactory trials. In this manner, I generated two independent population vectors for the full population (cells × time matrix each for the cue modalities). I obtained a pattern similarity index by calculating the Fisher-transformed Pearson correlation (r) between these two population vectors. This index provided the pattern similarity for both equivalent and different time points (for example, **Fig. 13a**). A positive value was interpreted as evidence for a reliable choice-direction encoding irrespective of the cue modality.

To estimate the mean performance values for the pattern

classification analysis, I randomly resampled the neurons (the same number of neurons as neural population analyzed) and computed the choice-direction selectivity in visual and olfactory trials. Neural responses were aligned to withdrawal onset from the central port (for a cue epoch), target-choice onset (for a reward epoch), and target-choice offset (for two return-epochs). For return-epoch responses, I analyzed neural responses before and after the animals left the target ports in preparation for the next trials (pre-return epoch: −400 to 0 ms before leaving a target port: post-return epoch: 0 to 400 ms after leaving a target port). Only trials where the animals directly returned from the target port to the central port for the next trial were included in the analysis. These data allowed us to compute the pattern similarity indices within an epoch or across two different epochs. To investigate choice-direction encoding during the epochs, I averaged the performance within each of the epochs (the cue, reward, pre-return and post-return epochs). To obtain a baseline performance, I averaged the classification performance during the baseline epoch, −400 to 0 ms before the cue onset. I also quantified the pattern similarity of the neural responses between two epochs (for simplicity, I here refer to these epochs as A-epoch and B-epoch) by

averaging the following two pattern classifications: pattern classification for A-epoch responses in visual trials and B-epoch responses in olfactory trials, and A-epoch responses in olfactory trials and B-epoch responses in visual trials (for example, **Fig. 13c**). I repeated the above processes 1,000 times to obtain a distribution of 1,000 different measurements of each pattern classification. To determine statistical significance, I compared a distribution obtained from 1,000 different pattern classification measurements within an epoch with a baseline distribution using the above described estimated *P* value. I considered zero to be a chance level instead of the baseline distribution when I verified the statistical significance of the classification across the epochs.

2.6.4. Decoding analysis of erroneous trials

I included 119 neurons recorded in sessions with a sufficient number of erroneous target-choices (at least 11 trials for both directions of target-choice) in all the analyses for erroneous trials. Due to the similarity of the choice-direction selectivity between the different cue-modalities in correct trials (**Fig. 10c** and **13a**), I computed the pattern similarity index using correct visual trials and erroneous olfactory trials to evaluate the influence of erroneous behavioral performance on the choice-direction encoding (**Fig. 13e**). In the erroneous trials, the animals chose the same target-port as the correct trials. To determine the statistical significance of pattern classification performance in correct and erroneous trials, the correct olfactory trials were downsampled to match the number of trials for the erroneous olfactory trials (**Fig. 13f**). To test whether the classification performance during each epoch decreased from the correct trials to erroneous trials, I subtracted the classification performance in the erroneous trials from that in the correct trials for each resampling. The distribution of the residual performance was compared with zero by using the estimated P value.

2.6.5. State-space analysis for population-level dynamics

To understand the population structure and its temporal changes between the cue and reward epochs, I performed the principal component analysis (PCA) (**Fig. 7**). For each of the epochs, I constructed 207 neurons × 4 conditions matrix (Cavanagh et al., 2018; Murray, 2017), in which columns contained trial-averaged z-scored firing rates of each neuron. The instantaneous firing rate of each neuron (estimated by spike counts in a 150 ms sliding window with 10 ms increment) was converted to a z-score by normalizing to the mean and standard deviation of its instantaneous firing rates during the baseline epoch. I then obtained time-averaged firing rates of the neurons each for the cue and reward epochs. By performing PCA on these datasets, I reduced the dimensionality of the PRC population from 207 neurons to two principal components (**Fig. 15b**). I independently performed this analysis for population responses during the cue and reward epochs to obtain the cue-epoch and reward-epoch subspaces.

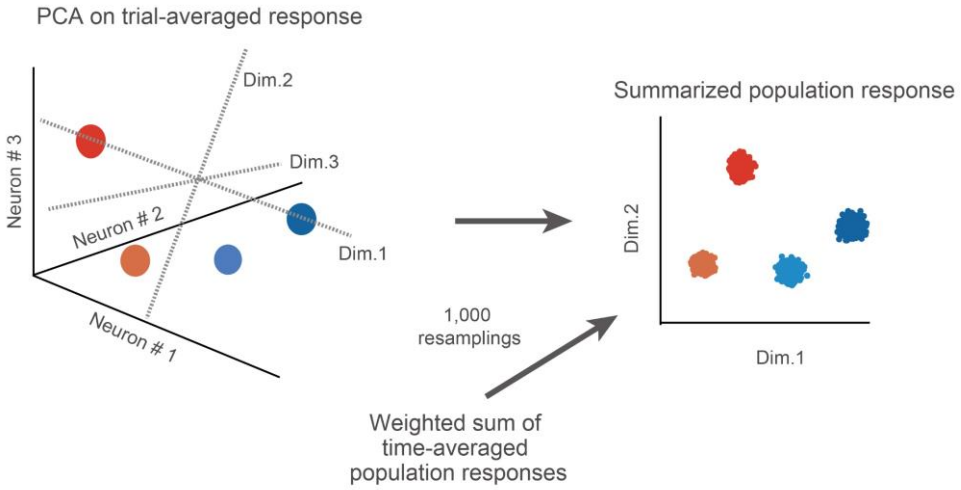

Figure 7 | Schematics drawing of the procedure of PCA.

For simplicity, I here show an example of performing PCA used this study on 3 neurons × 4 conditions matrix. As shown in the left, the PCA was performed on the trial-averaged population response across the different trial-conditions (shown by different colors). The population response in each trial-condition is represented as a point in a Euclidian space defined by the firings of the three neurons. The dimension which captures the largest variance of the population responses was defined as the first dimension, and the dimension orthogonal to the first dimension was defined as the second dimension. Also, the dimension which is orthogonal to these dimensions was defined as the third dimension. Since I used 207 neurons × 4 conditions matrix in the real analysis, which has the same sample size to this example plot (that is, the number of conditions), I obtained three dimensions capturing the responses of the neural population consisted of 207 neurons (Fig. 15b). I projected population responses in different subsets of trials onto these dimensions, by multiplying those responses by weighting value of each neuron obtained from the PCA and then summing them.

For data projections onto the above two-dimensional neural subspaces, I randomly selected 25 trials for each of the four conditions. Z-scored firing rates of each neuron were then obtained by normalizing the data to the mean and standard deviation of its firing rates during the baseline epoch. I averaged the z-scored firing rates of each neuron during each of three epochs (the cue, reward, and baseline epochs) to obtain 207 cells × 4 conditions matrix for each epoch. To visualize the population responses, I projected these data onto the two-dimensional PCA space. This allowed us to obtain a single point reflecting the entire population response for each of the four conditions. I repeated this procedure five times with different subsets of 25 trials, and this allowed us to reduce some degree of the variability among individual trials. To obtain the within-condition distance, I computed the mean of pairwise Euclidean distances for five points in each of the four conditions and then averaged those distances across the conditions to obtain a single value for the within-condition distance. To obtain the across-condition distance, I computed pairwise distances between two sets of five points obtained from two different conditions in the same subspace and then averaged them. This procedure was repeated for all possible combinations between two different

conditions of interest, and I then averaged those distances to obtain a single value for the across-condition distance. I also investigated how the representational geometry for the choices changed between different epochs (that is, the temporal shift of population responses in a neural subspace). This was achieved by computing the mean of pairwise distances between two sets of five points obtained from neural responses under a single condition in two different epochs. The mean distance on the first dimension was obtained for all trial conditions of interest and then averaged to produce a single value for the across-condition distance for the temporal shifts.

To visualize variability across different subsets of trials (**Fig. 15a** and **17a**) and test statistical significance, the above analysis was repeated 1,000 times with different subsets of resampled trials. The across-condition distances of the projections on corresponding subspaces (that is, cue-epoch responses onto cue-epoch subspace and reward-epoch responses onto reward-epoch subspace; **Fig. 15a**) were compared with a distribution of the within-condition distance using the above described estimated *P* value (**Fig. 15c**). Across-condition distances larger than within-condition distance indicated that different trial conditions were discriminated at the population level. For

projections onto the interchanged subspaces (that is, cue-epoch responses onto reward-epoch subspace and reward-epoch responses onto cue-epoch subspace; **Fig. 17a**), the across-condition distance for different choice-directions on the first dimension was computed in each modality and then averaged. I compared those distances with a distribution of within-condition distance on the first dimension by using the estimated *P* value (**Fig. 17b**). Similarly, I also projected baseline-epoch responses as negative controls (**Fig. 17b, 18a, and 20**). To investigate the importance of the temporal response patterns of individual neurons, I projected randomly shuffled data (**Fig. 17b** and **20**), where the correspondence between the cue-epoch responses and reward-epoch responses were shuffled among the neurons (**Fig. 18b**). I considered across-condition distances of the baseline-epoch responses to be a chance level when I evaluated the temporal shifts in representational geometry between the cue and reward epoch in a neural subspace (**Fig. 20a**).

To directly evaluate the contribution of individual neurons to the choice-direction encodings (**Fig. 19b**), I performed the following analysis. I first sorted all the neurons from ones with the highest magnitude of the weighting values on the first dimension of the cue or reward epoch. For these

differently sorted populations, I performed cluster projections onto the corresponding subspaces with increasing numbers of neurons. For precise evaluation of each neuron's contribution, rather than performing PCA on each of differently sized populations independently, I used the same projection data in **Fig. 15a** and **17a** (that is, the full population data) and replaced the weighting values of excluded neurons with zero. In each size of the population, the across-condition distance for different choice-directions on the first dimension was computed for each modality and then averaged. Those distances were then normalized to the distance obtained from the full population. I compared the distances from differently sized populations with those from the full population by the estimated P value. When the estimated P exceeded 0.05, I considered that number of neurons was sufficient to achieve the discriminability of the choice directions equivalent to the full population.

Chapter 3. Results

3.1. Fundamental response features of the PRC neurons

3.1.1. The PRC neurons are more sensitive to the animals' choice behavior than the cue-modality information

The rats were trained to perform a two-alternative forced-choice task where they chose a target port (left/right) associated with a presented cue to obtain the reward (**Fig. 8a–b**). The task performance was of a similar level regardless of the cue modality (mean correct rate in visual trials = 95.6 ± 5.5%; olfactory trials = 92.3 ± 4.3%). Spiking activities were recorded from the left PRC (n = 207 neurons; **Table 1**) during the task performance (37 sessions in five rats; **Fig. 9**).

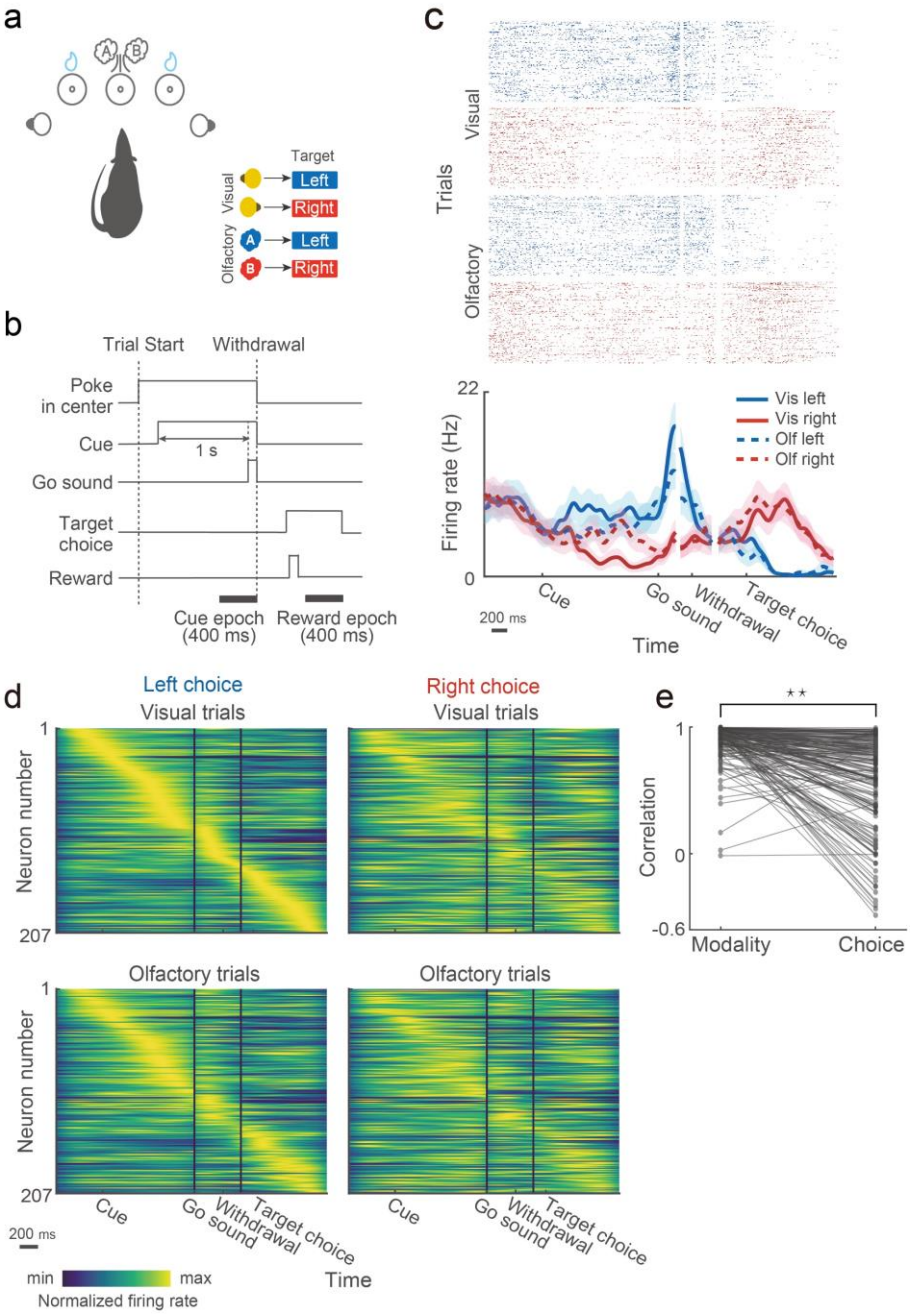

Figure 8 | Firing patterns of the PRC neurons in the two-alternative forced-choice task.

(**a**) Schematic drawing of the behavioral apparatus and the cue-target associative relationships. (**b**) Schematic of the task timeline. (**c**) Raster plot and peri-event time histogram showing the response of a representative neuron. Trial types are classified according to cue modality and target choice as follows: blue, left target-choices; red, right target-choices; solid line, visual trials; dashed line; olfactory trials. Neural

responses in correct trials were independently aligned to cue, withdrawal, and target-choice onset and then reconstructed because of variable time between them. Lines and shaded areas indicate mean and s.e.m., respectively. (**d**) Firing patterns across all the neurons (n = 207) for the different trial conditions. In each trial type, the mean firing rate of each neuron was normalized to its peak. For all trial types, the neurons were sorted by their peak firing time in visually-cued left choice trials (upper left). (**e**) Comparison of temporal firing patterns of individual neurons between the different modalities and choice directions. For comparison between different modalities, for each neuron, correlation coefficients were computed between peak-normalized firing rates in the visual left (upper left in d) and olfactory left trials (bottom left in d). For comparison between different choices, correlation coefficients were computed between peak-normalized firing rates in the visual left (upper left in d) and visual right trials (upper right in d). Nearly identical results were achieved when correlation coefficients were computed between the visual right and olfactory right trials and between the olfactory left and olfactory right trials (Two-sided Wilcoxon signed-rank test; mean correlation for different modalities = 0.872 ± 0.13, mean correlation for different choice-directions = 0.62 ± 0.358, $P = 1.515 \times 10^{-23}$).

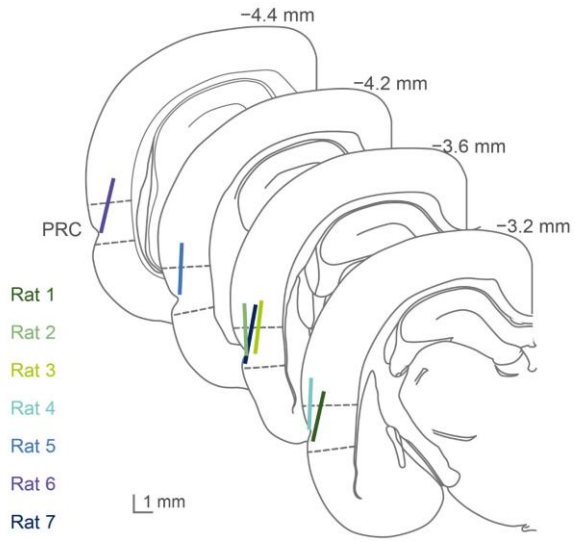

Figure 9 | The distribution of recoding sites in the PRC.

Coronal sections of the brain (adapted from Paxinos & Watson, 2007) indicating the tracks of the electrodes in each subject. Individual subjects were shown in different colors. Areas surrounded the dashed lines indicate the PRC. Rat 6 and 7 were used in the control experiments shown in Chapter 3.1.3.

Table 1 | Electrophysiological recordings in the individual animals.

Subject	Rat 1	Rat 2	Rat 3	Rat 4	Rat 5	Rat 6	Rat 7
Num. of neurons	22	93	23	33	36	62	43
Isolation quality (isolation distance, mean ± s.e.m.)	67.1 ± 96.4	52.3 ± 62.48	67.1 ± 96.4	40.1 ± 34.5	49.6 ± 28.1	47.2 ± 26.2	48.9 ± 72.2
Session firing rate (Hz, mean ± s.e.m.)	1.9 ± 1.6	2.5 ± 1.8	1.3 ± 1.6	1 ± 0.5	1.4 ± 0.9	2.2 ± 2.1	1.6 ± 1

As shown in **Fig. 8c**, the PRC neurons typically showed distinct temporal firing patterns in the left and right trials. To characterize how the PRC was activated by different trial conditions, I compared firing patterns among different cue-modalities and choices across the recorded neurons (n = 207 neurons). The neurons were sorted by their peak firing rates in visually-cued left choice trials (top left in **Fig. 8d**). As consistent with previous studies in other brain regions (Shiotani et al., 2018; Handa et al., 2017; Hwang et al., 2017; Akhlaghpour et al., 2016; Harvey et al., 2012; Fujisawa et al., 2008), the peak responses of the PRC neurons tiled the duration of a trial, suggesting flexible responses to multiple epochs of the task. The temporal response patterns across the neurons were well preserved between the cue modalities (comparison between the top and bottom in **Fig. 8d**) but much less so between the choice directions (comparison between the left and right in **Fig. 8d**). I found that the majority of the neurons showed more strongly correlated temporal response patterns between different modalities than between different choice directions (two-sided Wilcoxon signed-rank test; $P = 1.186 \times 10^{-24}$; **Fig. 8e**). These results suggest that firings of the PRC neurons are more sensitive to the animals' choice behavior than cue information.

3.1.2. Inputs from different sensory modalities evoke similar response patterns across the PRC neurons according to learned cue-target associative relationships

I thus quantified selective responses of the individual neurons to the different choice-directions by using ROC analysis, which compared firing rates of a neuron between different choice-directions and converted the difference into "choice-direction selectivity". Here, we defined "choice-direction selectivity" broadly as signals reflecting a chosen direction in each trial. The individual PRC neurons showed the choice-direction selectivity at different time points of the trial duration (**Fig. 10a**). In addition, each neuron often showed such encodings at the time points other than its peak selectivity, suggesting that the individual neurons flexibly respond to multiple epochs of the task. I found two epochs where the choice-direction selectivity in both modalities reaches its peak (**Fig. 10b**), the cue epoch (−400 to 0 ms before withdrawal from the central port) and reward epoch (200 to 600 ms after choice). Many neurons encoded the choice-direction information during these epochs (**Fig. 10c**; 51.21% and 70.53% of the neurons showed significant selectivity in the cue and reward epochs, respectively). I observed a slight bias toward ipsilateral

choice in the cue epoch (two-sided sign test; mean visual choice-direction selectivity = 0.006 ± 0.124, P = 0.889; mean olfactory choice-direction selectivity = 0.025 ± 0.102, $P = 5.104 \times 10^{-4}$) but no bias in the reward epoch (two-sided sign test; mean visual choice-direction selectivity = −0.026 ± 0.154, P = 0.211; mean olfactory choice-direction selectivity = −0.021 ± 0.154, P = 0.331). To further characterize the ipsilateral bias in the cue epoch, I directly compared the magnitude of selectivity between the ipsilateral-selective and contralateral-selective neurons. In both modalities, the magnitude of the selectivity was not significantly different (two-sided Wilcoxon rank-sum test; P = 0.48 for visual choice-direction selectivity, P = 0.07 for olfactory choice-direction selectivity). These results show no reliable evidence for biased choice-direction encodings in the PRC, which is in line with recent findings in other cortical areas (Steinmetz et al., 2019; Raposo et al., 2014). The choice-direction selectivity was highly consistent across the cue modalities during both epochs (r = 0.593, $P = 5.180 \times 10^{-21}$ for the cue epoch; r = 0.858, $P = 2.837 \times 10^{-61}$ for the reward epoch; **Fig. 10c**), and the PRC neurons were not tightly clustered as a choice-direction selective subpopulation and the others but rather showed the graded selectivity as reported in other cortical areas

(Siniscalchi et al., 2019; Raposo et al., 2014). The neurons which showed significant selectivity across both modalities were sparser in the cue epoch (26% of selective neurons) than in the reward epoch (48% of selective neurons), but I found that the neurons classified as non-selective during the cue epoch (48.79%, 101 of 207 neurons) showed a moderate correlation between the cue modalities ($r = 0.357$, $P = 2.505\times10^{-4}$; inset of **Fig. 10c**). This suggested even such non-selective neurons might convey a fraction of the choice-direction information. Altogether, these results suggest that sensory inputs from different modalities evoke similar response patterns across the PRC neurons according to learned cue-target associative relationships.

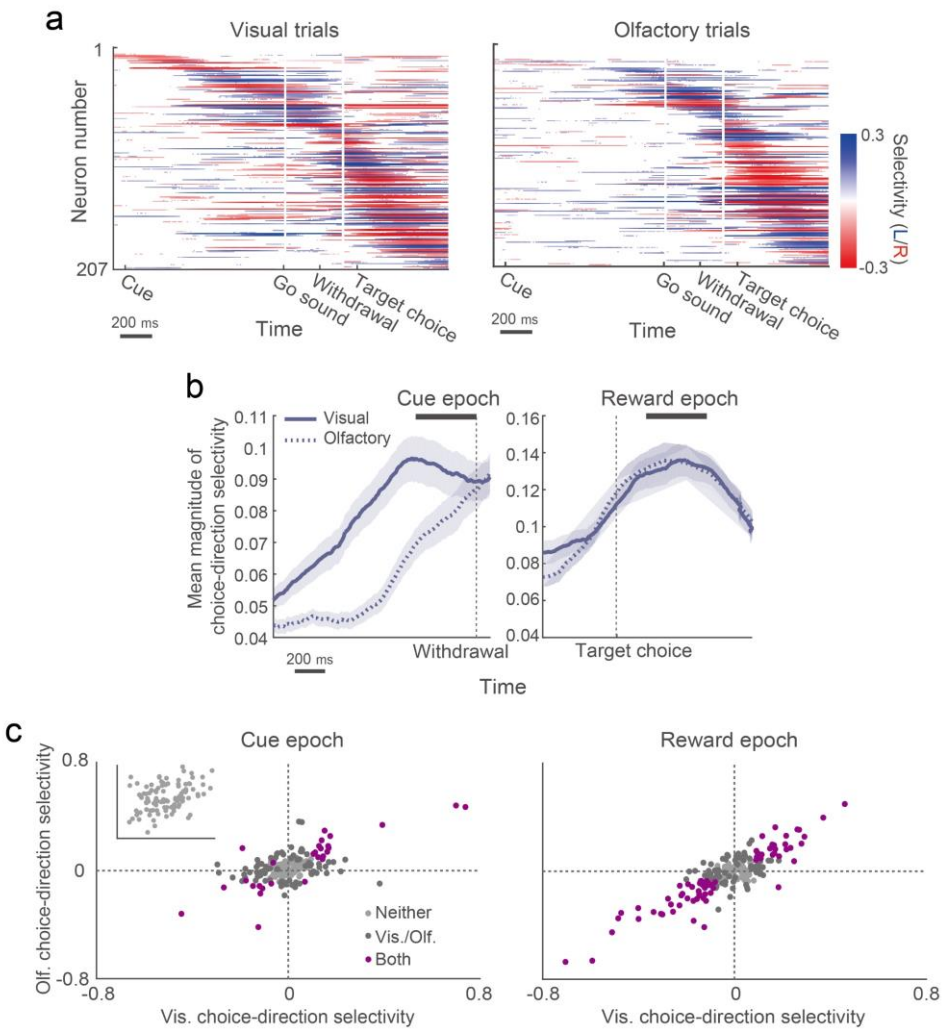

Figure 10 | Choice-direction selectivity of the individual PRC neurons in different epochs of the task.

(**a**) Temporal patterns of choice-direction selective responses of the PRC neurons (n = 207) in correct visual and olfactory trials. Colors indicate selectivity to the left (blue) or right (red) choice. In each modality, neurons were sorted according to the time of their peak selectivity. Only segments with significant selectivity are shown (P < 0.05; 1,000 permutations). (**b**) Time course of the choice-direction selectivity magnitude in visual (solid line) and olfactory (dashed line) trials averaged across all the neurons. Neural responses around the withdrawal onset (left) and target-choice onset (right) are shown. Lines and shaded areas indicate mean and s.e.m., respectively. (**c**) Scatter plots showing the choice-direction selectivity of the neural population during the cue (left) and reward (right) epochs (n = 207 neurons). Each point corresponds to values of a single neuron. Colors indicate significance (P< 0.05;

1,000 permutations): light gray, no selectivity; deep gray, significant in either cue modality; purple, significant in both cue modalities. Inset, the choice-direction selectivity of the non-selective neurons (n = 101) in the cue epoch.

3.1.3. Choice directions better explained neural responses in the PRC than major confounding variables

A potential caveat in the above conclusion, however, is that the choice-direction selectivity in the PRC can be attributed to some fundamental behavioral or contextual variables such as body posture, non-orienting movements, and spatial view (Musall et al., 2019; Steinmetz et al., 2019; Krumin et al., 2018; Wang et al., 2018; Akhlaghpour et al., 2016; Erlich et al., 2011). To evaluate the possible influence of those fundamental variables, I performed two control experiments. First, I monitored head angles of the animals (n = 2) during neural recordings (**Fig. 11a–c**) using a head-mounted accelerometer (Meyer et al., 2018). To quantify the influence of body posture and view angle on the PRC neural responses (n = 105), I compared prediction performance between linear-regression models with choice and x-axis (interaural axis) head angle by computing correlation between the neural responses and the model prediction across trials (**Fig. 11d**). The performance of the model with choice was higher than the model with x-axis head angle in both of the cue and reward epochs by 4.28% ± 10.98% (m.a.d) and by 32.07% ± 34.8% (m.a.d), respectively. I found that responses of the majority of the

PRC neurons were better explained by the choice than the x-axis head angle (two-sided sign test; cue epoch, $P = 0.019$; reward epoch, $P = 1.365\times10^{-7}$). Second, a delay period was inserted between the choice onset and the reward onset to dissociate the influence of anticipatory licking behavior (Yoshizawa et al., 2018) and spatial view (position) from the choice-direction selectivity in the reward epoch. I found that many of the neurons (69.52%, 73 of 105 neurons) encoded choice-direction after the onset of the reward (0 to 400 ms after reward onset) in accordance with the reward-epoch responses shown in **Fig. 10c**. The majority of these selective neurons (71.23%, 52 of 73 neurons) showed stronger selectivity after the onset of the reward than during the reward delay period (two-sided sign test; median difference in the magnitude of selectivity = 0.08, $P = 3.713\times10^{-4}$; **Fig. 11e**). Although the other neurons (28.77%; 21 of 73 neurons) showed stronger selectivity during the reward-delay period than after the reward onset, the size of such bias (that is, the difference in the magnitude between these periods) was relatively small (0.058 ± 0.061; $n = 21$ neurons) as compared to the bias to the reward onset (0.159 ± 0.122; $n = 52$ neurons). Taken together, these results suggest that fundamental variables such as body posture, non-orienting movements, and

spatial view themselves are not major factors for the choice-direction encodings in the PRC.

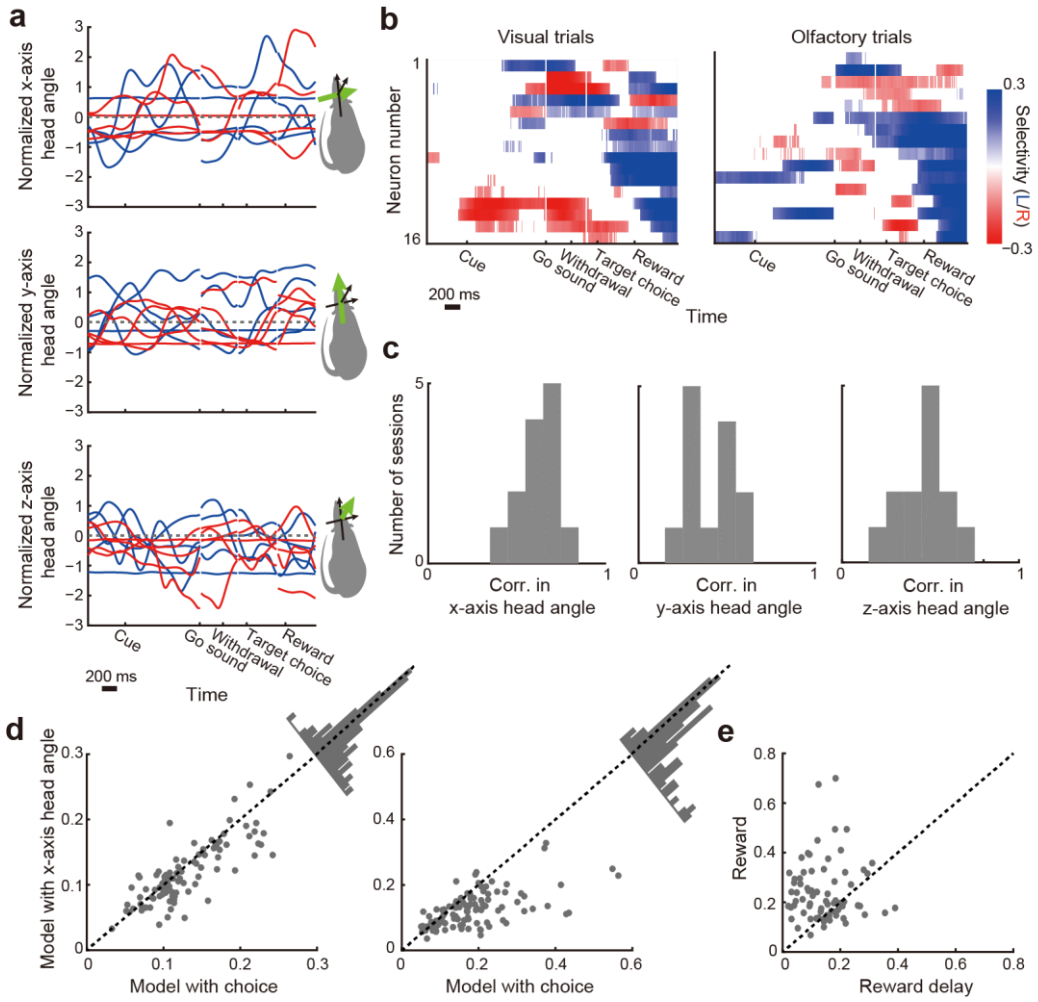

Figure 11 | Influence of fundamental behavioral and contextual factors on choice-direction encodings in the PRC.

(**a**) Diverse patterns of head angles of a rat in left (blue) and right (red) trials of an example session (463 trials). Traces represent estimated gravity components of accelerometer signals (Methods) in 5 trials randomly sampled for each direction of the target choices. (**b**) Choice-direction selectivity of neurons (n = 16) recorded in the example session shown in a. Only segments with significant selectivity are shown (P < 0.05; 1,000 permutations). For each modality, neurons were sorted according to their peak selectivity. (**c**) Correlations of head angles between the cue and reward epochs always showed positive values, suggesting no temporal inversion of body posture (13 sessions from two rats). (**d**) Comparison of prediction performance between linear-regression models with the choice direction and the x-axis head angle (n = 105 neurons from two rats) in the cue epoch (left) and the reward epoch (right). Those models also included the y-axis head angle, z-axis head angle, and reaction time as explanatory variables. For each neuron (shown by a point), the firing rate

during an epoch was independently predicted by the two models. The performance of the models was evaluated by computing correlation coefficients between the neural responses and the model prediction across trials. The better model to explain the neural responses was determined by the difference in correlation values between the models (the distributions are shown by histograms). (**e**) Comparison of the magnitude of the choice-direction selectivity between the reward epoch and the reward-delay epoch (0 to 400 ms after the target-choice onset). Neurons with significant choice-direction selectivity ($P < 0.05$; 1,000 permutations) during the reward epoch were included in this analysis ($n = 73$ of 105 neurons).

3.2. Temporal dynamics of choice-direction encodings in the PRC

3.2.1. Individual neurons flexibly encoded different choice-directions at multiple time-points of the trial duration

Thus far, I showed that the PRC neurons encoded the choice directions across the different cue modalities and that such signals were apparent at multiple epochs of the task (**Fig. 10** and **11**). Given the reduced correlation of temporal response patterns between the different choices (**Fig. 8d–e**), it is possible that the individual neurons flexibly tuned to different choices at different time-points of the trial duration. To characterize how each neuron represented the choice directions over the trial duration, I classified the neurons into two groups based on their peak selectivity: left-selective and right-selective neurons. As shown in **Fig. 12a**, I found similar numbers of selective neurons for both choice-directions. As expected, individual neurons showed selectivity to the opposite choice direction in time points other than their peak responses. Remarkably, when I sorted these neurons by their peak responses to the opposite choice (that is, left-selective neurons by right peaks and right-selective neurons by left peaks), response patterns nearly tiling the entire trial duration appeared (**Fig. 12b**). These results suggested flexible

engagements of individual neurons for different choice-directions rather than the recruitment of distinct subpopulations for each choice-direction.

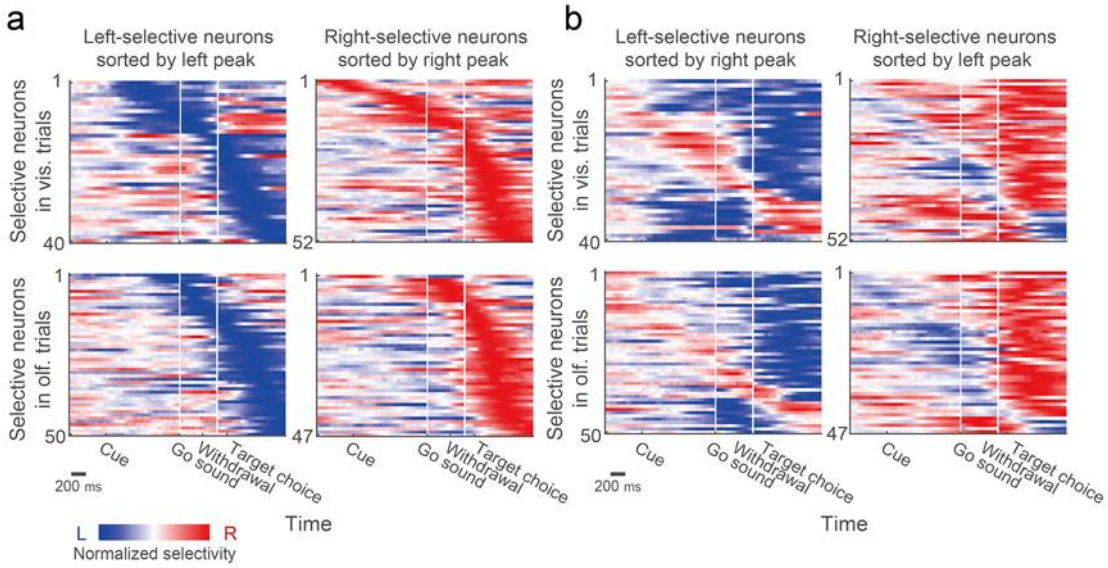

Figure 12 | Time-varying choice-direction selectivity in the individual neurons.
(**a**) Temporal response patterns of left-selective and right-selective subpopulations. In each modality, neurons were classified by their peaks of significant choice-direction selectivity (Fig. 10a). The selectivity of each neuron was normalized to its peak. The neurons were sorted according to the time of their peak selectivity. To visualize the entirety of time-varying selectivity, all segments with and without statistical significance are shown. (**b**) Same as in a, except for that the neurons were sorted by their peak selectivity to the opposite choice direction.

3.2.2. Dynamic changes of choice-direction encodings in the PRC were aligned to between the cue and reward epochs

I next sought to understand how such dynamic neural encoding patterns in the PRC appear and evolve through the trial duration as a population. A time-resolved pattern analysis (Spaak et al., 2017; Stokes et al., 2013; **Methods**) was performed to visualize the temporal evolution of the choice-direction encoding patterns across the PRC neurons (n = 207). Given the overall correlation of the choice-direction selectivity between the cue-modalities during the epochs where such encodings peak (**Fig. 10b–c**), I focused on modality-independent encoding patterns. The population response pattern evolved with two time-stable states (**Fig. 13a**). An encoding pattern was sustained during the presentation of the cue and was followed by a transient pattern during the movements towards the target ports. Soon after the rats chose a target port, the encoding pattern settled again into a stable state. To test for reliability of such encodings, I computed the mean performance of the classifier during the cue and reward epochs and compared them with a baseline epoch (−400 to 0 ms before the cue onset). As shown in **Fig. 13b**, the choice directions were decoded during both epochs above chance level (cue

epoch: $P \approx 0.002$; reward epoch: $P < 0.001$). Importantly, the encoding patterns were substantially inverted between the cue and reward epochs (scatter plots in **Fig. 13a**), indicating that the choice directions associated with the higher firing rates of individual neurons were the opposite between these epochs. The mean classification performance across those epochs revealed reliably inverted encoding patterns ($P < 0.001$; **Fig. 13c**). It is noteworthy that the inverted state was time-stable (**Fig. 13a**). This indicates that the time-varying encodings of the choice directions which I found in the previous section (**Fig. 12b**) are explicitly aligned to between the cue and reward epochs. In other words, the inverted encodings might be a form of coherent representation across different epochs of a given task, which is mediated by the individual PRC neurons.

However, it is still possible that the inverted encoding patterns were due to the reversal of orienting movements between the cue and reward epochs. To directly test this, I analyzed neural responses during two non-overlapping epochs before and after the animals left the target ports in preparation to the next trials (**Fig. 14**): the pre-return (−400 to 0 ms before the choice offset) and post-return epochs (0 to 400 ms after the choice offset).

These epochs did not show the equivalent level of inverted patterns to that of the cue epoch (cue × pre-return epochs: $P \approx 0.016$; cue × post-return epochs: $P \approx 0.1858$; comparison between cue × reward epochs and cue × pre-return epochs: $P \approx 0.023$; **Fig. 13c**) despite the fact that the choice-direction information was robustly represented during both pre-return and post-return epochs ($P < 0.001$; **Fig. 13d**). These results indicated little influence of orienting movements on the dynamic choice-direction encoding patterns.

I also asked whether the behavioral performance affect the neural responses by performing the pattern classification analysis with correct visual and erroneous olfactory trials ($n = 119$ neurons with a sufficient number of erroneous trials; **Fig. 13e**). As shown in **Fig. 13f**, the mean classification performance during both epochs was the chance level in erroneous trials (error cue: $P \approx 0.1389$; error reward: $P \approx 0.1349$). For an accurate comparison, the classification performance for correct trials was obtained from the visual and downsampled olfactory trials (**Methods**). After the downsampling, the mean classification performance was still above chance for the reward epoch but did not reach significance in the cue epoch (correct cue: $P \approx 0.073$; correct reward: $P < 0.001$), suggesting higher trial-by-

trial variability in the cue epoch. I tested whether the classification performance during each epoch decreased from the correct trials to the erroneous trials and found a significant reduction only in the reward epoch (cue: $P \approx 0.5385$; reward: $P < 0.001$). These different results suggest distinct neural computations underlying the choice-direction encodings in these epochs.

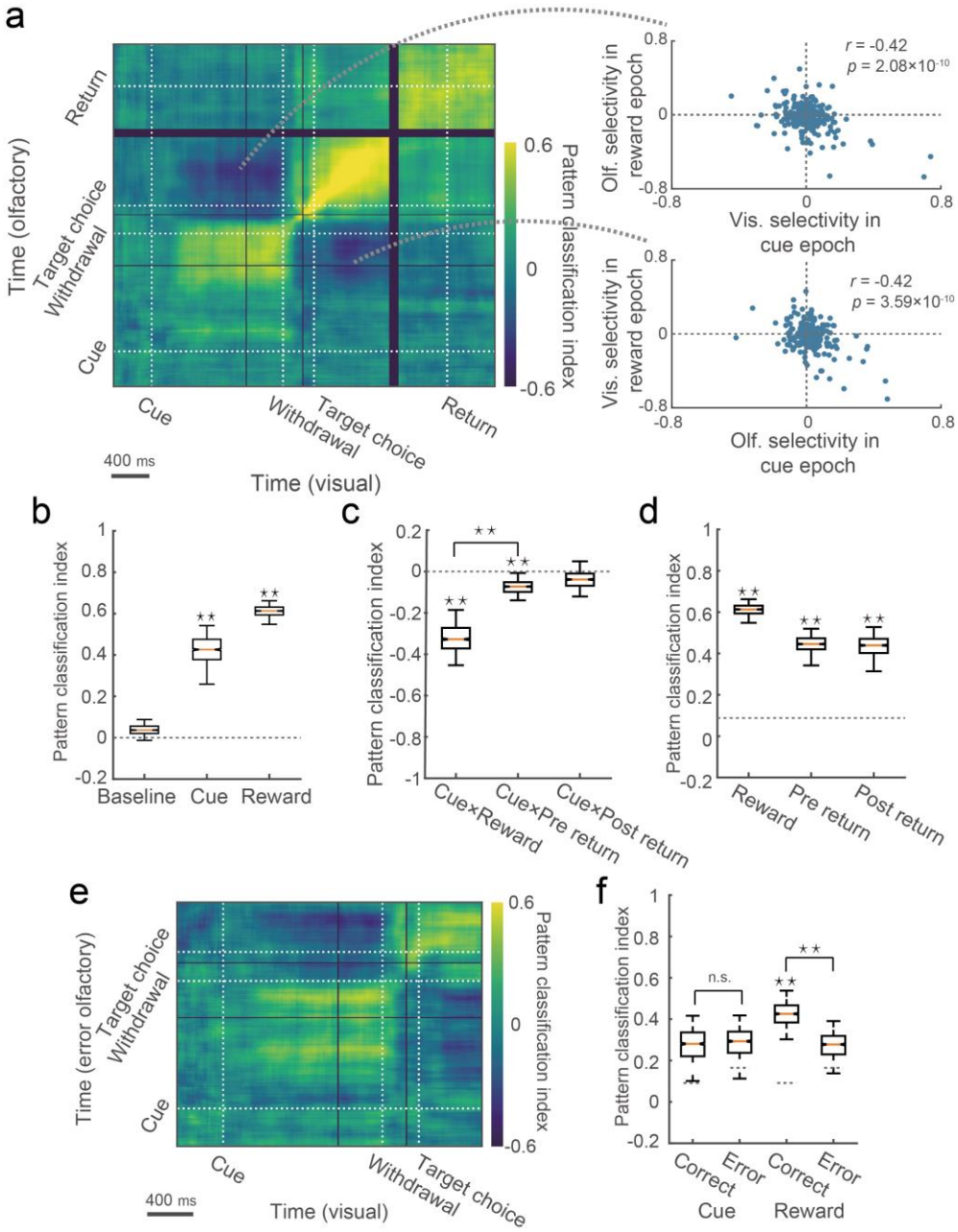

Figure 13 | Time-resolved pattern analysis for temporal changes of the choice-direction selectivity.

(a) Performance of the pattern classification analysis (left). White lines correspond to the onset times of cue, withdrawal, target choice, and return movements to the central port (target-choice offset). I trained a classifier using neural responses in correct visual trials to discriminate choice directions and tested them with neural

responses in correct olfactory trials (n = 207 neurons). Temporal inversions of choice-direction selectivity between the cue and reward epochs are shown by scatter plots (right). (**b**) Mean classification performance during the baseline, cue, and reward epochs. (**c**) Mean classification performance across two different epochs. (**d**) Mean classification performance during the reward, pre-return, and post-return epochs (Fig. 14). The dashed line indicates the 97.5th percentile values of the baseline distribution shown in b. (**e**) A classifier tested with erroneous olfactory trials (n = 119 neurons). (**f**) Mean classification performance in erroneous trials compared with correct trials. Dashed lines indicate the 97.5th percentile values of the baseline distributions in the correct and erroneous trials. In box plots: orange line, median; box limits, 25th and 75th quartiles; notch limits, (1.57 × interquartile range)/$\sqrt{n}$; whiskers, 95th percentile range (two-sided) of the distribution. Asterisks indicate statistical significance based on estimated P values (P < 0.05; Methods), and n.s. indicate insignificance.

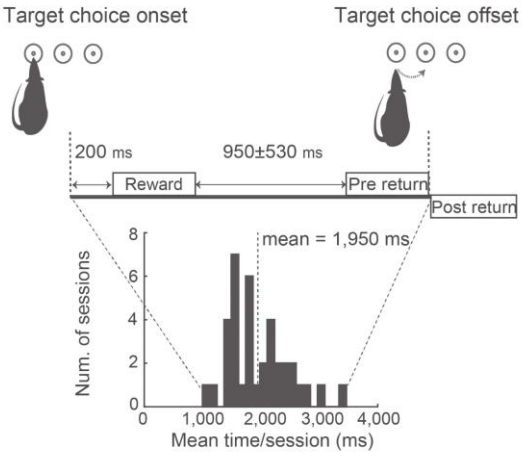

Figure 14 | Temporal relationships among the reward, pre-return, and post-return epochs.

The rats typically stayed in the target port 1950 ± 530 ms (mean ± s.d.) after the target-choice onset (37 sessions in five rats). The reward and pre-return epochs were separated by a period ranging 950 ± 530 ms (mean ± s.d.). Therefore, there were rare temporal overlapping between the reward epoch and the pre-/post-return epochs.

3.3. Analysis for population-encoding structure in relation to single-neuron representations

3.3.1. Population encodings during the cue and reward epochs

To investigate how such coherent response patterns appeared and worked under the entire population structure, I identified neural subspaces for the cue and reward epochs by performing the principal component analysis (PCA). Since the focus was to compare population response patterns between the different epochs, PCA was applied to time-averaged cue-epoch and reward-epoch responses across conditions (that is, PCA on neurons × conditions matrix for each epoch) (Cavanagh et al., 2018; Murray et al., 2017). This allowed us to clarify the population-encoding structure derived from the cue-epoch responses and reward-epoch responses and directly investigate the interrelationship between them. I projected the cue-epoch and reward-epoch responses onto the first two dimensions of the cue-epoch and reward-epoch subspaces (**Fig. 15a–b**). The different choices and cue modalities were clearly separated when I projected the neural responses onto the corresponding neural subspaces (**Fig. 15a,** cue epoch in left; reward epoch in right). Although I observed highly correlated choice-direction selectivity between the visual

and olfactory cues (**Fig. 10c**), modality information was evident in these plots. In both epochs, the first and second dimensions mainly captured the difference of the choice directions and the cue modalities, respectively. I quantified separation among the four different conditions in those plots by comparing the average distance among responses under different conditions (across-condition distance) with the average distance among responses under the same conditions (within-condition distance). The former distance indicates the discriminability of the different conditions and the latter indicates the variability of the population responses within each condition. The results revealed that the across-condition distance was significantly larger than the within-condition distance in both projections, indicating reliable encodings of the different conditions during both epochs ($P < 0.001$; **Fig. 15c** and **Methods**).

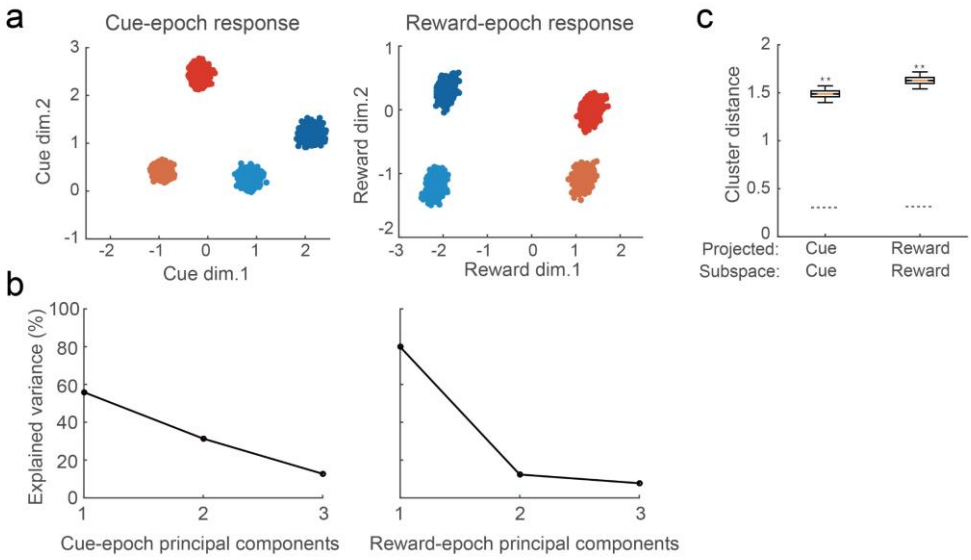

Figure 15 | The PRC population represented the choice-direction and cue-modality information during the cue and the reward epochs.

(**a**) Population responses during cue and reward epochs projected onto the first two dimensions of cue-epoch and reward-epoch subspaces. Blue, left target-choice in visual trials; pale blue, left target-choice in olfactory trials; red, right target-choice in visual trials; orange, right target-choice in olfactory trials. Each point corresponds to the population response in a subset of trials. (**b**) Percentage of the cue-epoch response variance explained by the cue-epoch principal components (left) and percentage of the reward-epoch response variance explained by the reward-epoch principal components (right). The cue-epoch and reward-epoch subspaces shown in Fig. 15–18 were defined as the first two principal components, which captured 84.36% and 89.18% of the data variance of the cue-epoch and reward-epoch responses, respectively. (**c**) Comparisons between across-condition distances and within-condition distances obtained from projections onto corresponding subspaces. Dashed lines indicate the 97.5th percentile ranges of within-condition distances. In box plots: orange line, median; box limits, 25th and 75th quartiles; notch limits, (1.57 × interquartile range)/$\sqrt{n}$; whiskers, 95th percentile range (two-sided) of the distribution. Asterisks indicate statistical significance based on estimated P values ($P < 0.05$; Methods).

3.3.2. Neural weights were widely distributed across the PRC neurons

I also determined whether these neural subspaces depended on the entire neural population or only a fraction of the neurons. I found that neural weights were highly distributed across the neurons (**Fig. 16**) with no neurons showing zero weight. This suggests that these subspaces reliably reflect coordinated response patterns across the PRC neurons.

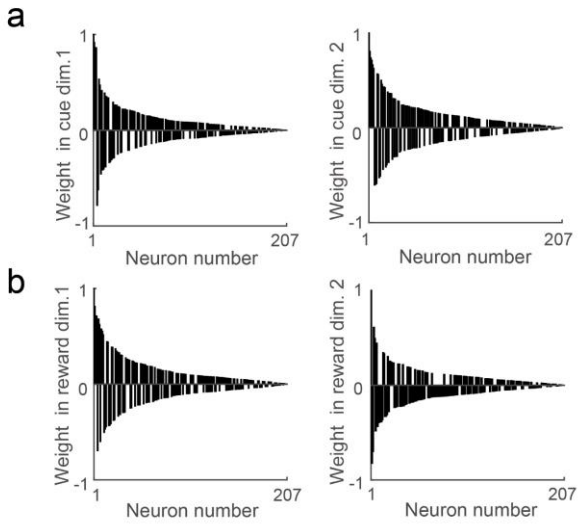

Figure 16 | Distributions of the neural weights in each dimension.
(**a**) Weights of individual neurons in the first two dimensions of the cue-epoch subspace shown in Fig. 15a. The values were normalized by the magnitude of the highest weighting value and were ordered by magnitude. (**b**) The same as a but for the reward-epoch subspace.

3.3.3. Interrelationships between the cue-epoch and reward-epoch responses

To directly investigate the relationship between the cue-epoch and reward-epoch responses, I projected the population responses onto the interchanged neural subspaces (that is, the cue-epoch responses onto the reward-epoch subspace and the reward-epoch responses onto the cue-epoch subspace) (Parthasarathy et al., 2017; Elsayed et al., 2016). The results showed that the choice directions but not the cue modalities were separable through the epochs (**Fig. 17a**, cue-epoch responses onto reward-epoch subspace in left; reward-epoch responses onto cue-epoch subspace in right). To test the reliability of the choice-direction discriminability sustained across the epochs, I compared the across-condition distance for different choice-directions on the first dimension with within-condition distance. As shown in **Fig. 17b,** in both subspaces, I found cluster separations above chance (reward-epoch responses in cue-epoch subspace: $P < 0.001$; cue-epoch responses in reward-epoch subspace: $P < 0.001$), revealing that the choice-direction information was reliably sustained between those different epochs.

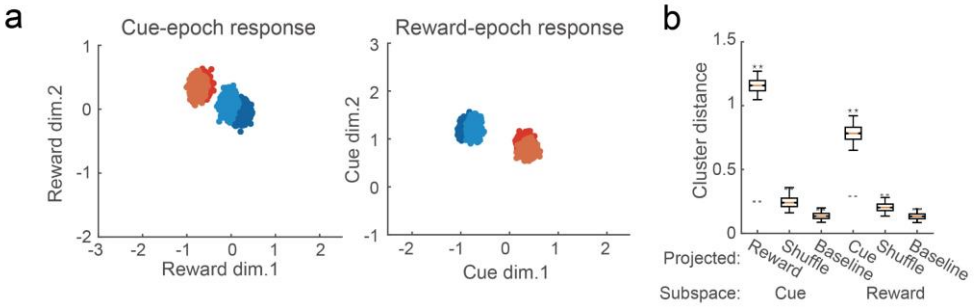

Figure 17 | Choice-direction encodings were sustained between the cue and reward epochs.

(**a**) Population responses during cue and reward epochs projected onto the interchanged subspace. The cue-epoch responses were projected onto the reward-epoch subspace (left), and the reward-epoch responses were projected onto the cue-epoch subspace (right). Blue, left target-choice in visual trials; pale blue, left target-choice in olfactory trials; red, right target-choice in visual trials; orange, right target-choice in olfactory trials. Each point corresponds to the population response in a subset of trials. (**b**) Comparisons between across-condition distances and within-condition distances obtained from projections onto interchanged subspaces shown in a and Fig. 18. Dashed lines indicate the 97.5th percentile ranges of within-condition distances. In box plots: orange line, median; box limits, 25th and 75th quartiles; notch limits, (1.57 × interquartile range)/$\sqrt{n}$; whiskers, 95th percentile range (two-sided) of the distribution. Asterisks indicate statistical significance based on estimated P values ($P < 0.05$; Methods).

I also projected the neural responses during the baseline epoch onto the same neural subspaces as negative controls (**Fig. 18a**). This analysis revealed no significant cluster separations ($P \approx 0.998$ for cue-epoch subspace; $P \approx 1$ for reward-epoch subspace; **Fig. 17b**), indicating no reliable encodings of the choice-direction information. I then tested whether the temporal response patterns of the individual neurons contributed to the observed discriminability by projecting randomly shuffled data where the temporal response patterns of the individual neurons were collapsed (**Fig. 18b**). The results showed no significant separations ($P \approx 0.998$ for shuffled reward-epoch responses in cue-epoch subspace; $P \approx 0.999$ for shuffled cue-epoch responses in reward-epoch subspace; **Fig. 17b**), suggesting that the coherence between the cue and reward epochs at the single-neuron level was critical for the discriminability observed at the population level.

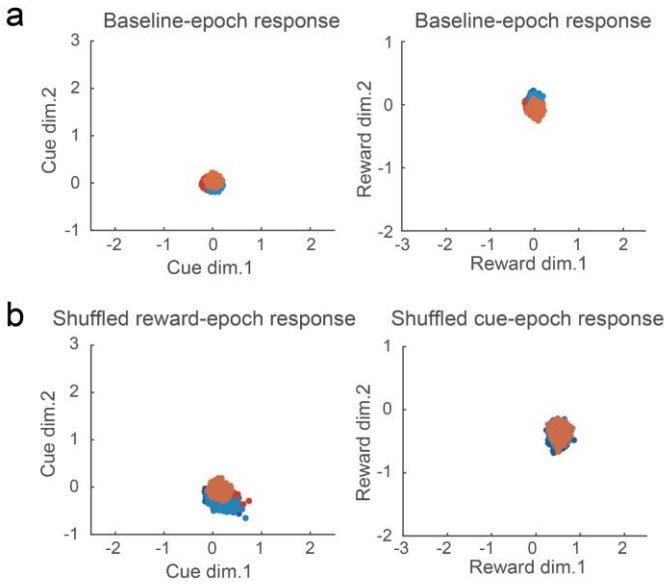

Figure 18 | Projections of the baseline-epoch and temporally shuffled responses onto the cue-epoch and reward-epoch subspaces.

(**a**) Population responses during the baseline epoch (−400 to 0 ms before the cue onset) projected onto the cue-epoch and reward-epoch subspaces. Blue, left target-choice in visual trials; pale blue, left target-choice in olfactory trials; red, right target-choice in visual trials; orange, right target-choice in olfactory trials. Each point corresponds to the population response in a subset of trials. (**b**) Projections of shuffled data onto interchanged subspaces. The shuffled data were generated by randomly shuffling the order of neurons in the projection data shown in Fig. 15a and 17a. The shuffled reward-epoch responses were projected onto the cue-epoch subspace (left), and the shuffled cue-epoch responses were projected onto the reward-epoch subspace (right). The within-condition and across-condition distances obtained from a and b were shown in Fig. 17b and 20a.

3.3.4. Dynamic coordination of the PRC neurons supports coherent choice-direction encodings across the cue and reward epochs

It might be possible that only a handful of neurons had strongly contributed to both cue-epoch and reward-epoch subspaces, thus resulting in the shared neural dimensions (that is, the first dimensions which consistently discriminated the choice directions) shown in **Fig. 17a**. However, this was not the case. As shown in **Fig. 19a**, the plot of the values of neural weights in the first dimensions of the cue-epoch and reward-epoch subspaces showed neither explicit clusters nor a tight correlation but rather exhibited a continuous distribution with a moderate correlation (r = 0.337, P = 7.12×10^{-7}). This suggests that many neurons dynamically changed their contribution to the shared dimensions across the epochs, while a degree of temporal coherence supporting those shared dimensions was maintained at the population level. Diverse relationships of neural weights of the cue and reward epochs were observed even among neurons with significant choice-direction selectivity (computed using ROC analysis in **Fig. 10c**) across the epochs (blue points in **Fig. 19a**). This result indicated heterogeneity of temporally coherent single-neuron responses in their contributions to the entire population structure. In

other words, each of those neurons might play a unique role in the population encodings under different computations.

To further establish population-level encoding (Siniscalchi et al., 2019; Mendoza-Halliday & Martinez-Trujillo, 2017; Morcos & Harvey, 2016; Raposo et al., 2014) in the PRC, I directly examined the distribution of choice-direction information over individual neurons. I asked what fraction of the neurons is necessary to achieve choice-direction discriminability (that is, the across-condition distance for different choice directions on the first dimension of a given epoch) which is equivalent to the entire population (**Methods**). The number of neurons incorporated was gradually increased, beginning with ones with the highest magnitude of the weighting values on the first dimension of the cue or reward epoch (**Fig. 19b**). As expected from the shape of the distribution in **Fig. 16**, when the neurons were sorted by the cue-epoch weights, the choice-direction discriminability in the cue subspace steeply increased with the incorporation of neurons (left in **Fig. 19b**). However, the top 73.43% of the neurons were necessary to achieve the discriminability as high as the entire population. Similarly, when the neurons were sorted by the reward-epoch weights, the discriminability in the reward subspace reached

as high as the full population after including 85.02% of the neurons (right in **Fig. 19b**). These results support population-level representations in which information is distributed across a number of individual neurons in the PRC. On the other hand, the choice-direction discriminability more gradually increased for the epochs to which the orders of neurons were not aligned (**Fig. 19b**), highlighting the dynamic changes in the neural weights between the epochs observed in **Fig. 19a**. I found that nearly all the neurons were necessary to achieve the discriminability as high as the full population (neurons sorted by cue-epoch weights, 100%; neurons sorted by reward-epoch weights, 97.58%), indicating that the choice-direction representations across the two epochs were distributed widely over the entire population. However, the mean discriminability in the epochs in which the neurons were indirectly sorted more steeply increased than the linear increase which is expected when the neurons were added in a random order (two-sided Kolmogorov-Smirnov test; cue epoch, $P = 5.721\times10^{-15}$; reward epoch $P = 2.078\times10^{-5}$). As shown in **Fig. 19b**, by incorporating a small subset of the neurons (~ three neurons), those curves deviated from the linear increase and the deviation was sustained through almost all the parts of the curves. Therefore, the

choice-direction information in the cue and reward epochs was highly distributed across the neurons, but its coherence was reliably sustained at the population level.

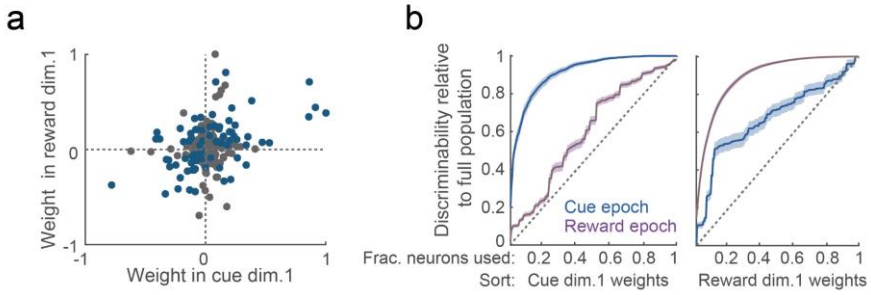

Figure 19 | Choice-direction information in the cue and reward epochs were widely distributed over the PRC population.

(**a**) Correlation between the neural weights in the first dimensions of the cue and reward subspaces shown in Fig. 16. Blue points, neurons with significant choice-direction selectivity ($P < 0.05$; Fig. 10) across the cue and reward epochs. (**b**) Choice-direction discriminability by the neural population with increasing numbers of neurons. Neurons were arranged by the weighting value on the first dimension of the cue epoch (left) or the reward epoch (right). Values were normalized to the discriminability of the full population. Lines and shaded areas represent mean and 95th percentile range, respectively. Dotted lines indicate a linear increase expected by random incorporation of the neurons.

3.3.5. Efficient encoding of choice directions and different task-epochs by the PRC population

As shown in **Fig. 15a** and **17a**, the population response patterns representing the choice directions were substantially inverted on the first dimension when I compared the cue-epoch responses and reward-epoch responses in the same neural subspace (for example, comparison between the left plot in **Fig. 15a** and the right plot in **Fig. 17a**). In contrast, when the population responses from one of these epochs were projected onto the cue-epoch and reward-epoch subspaces (for example, comparison between the left plot in **Fig. 15a** and the left plot in **Fig. 17a**), the relative positions of the different choice-directions were preserved, indicating that the directions (that is, signs) of the first dimensions were consistent. Therefore, these results suggested that information of the different epochs was also represented in these shared first dimensions by flexible changes in the representational geometry. The inverted geometry was consistent with the dominant temporal response pattern observed in **Fig. 13a**. To test the reliability of the temporal inversions, in the first dimensions of each subspace, I computed the average distance between population responses under the same conditions in the different

epochs (for example, distance from cue-epoch responses to reward-epoch responses in the cue subspace) (**Methods**). I compared those distances with an average distance from one of those epochs to the baseline epoch (for example, distance from cue-epoch responses to baseline-epoch responses in the cue subspace), which is equivalent to the range of chance-level cluster shifts caused by the absence of choice-direction representations (that is, overlapped clusters in **Fig. 18a**). As shown in **Fig. 20a**, the results showed larger task-epoch dependent shifts of the representational patterns than expected by chance ($P < 0.001$ for cue-epoch subspace; $P < 0.001$ for reward-epoch subspace). The discriminability was diminished when the temporal patterns of individual neural responses were collapsed by data shuffling ($P \approx 0.986$ for shuffled reward-epoch responses in cue-epoch subspace; $P \approx 0.999$ for shuffled cue-epoch responses in reward-epoch subspace). These results suggested that the coherent response patterns at the individual neurons mediated flexible changes for task-epoch representations. Finally, I asked how these flexible encodings for the cue and reward epochs (**Fig. 20a**) were related to the coherent choice-direction encodings across those epochs (that is, across-condition distance in **Fig. 17b**). I compared the variability of the choice-

direction discriminability and the temporal shift distance across subsets of trials (**Fig. 20b**). I found that transition of the population response between the cue and reward epochs resulted in a high correlation between the two values (r = 0.719, $P = 1.369 \times 10^{-159}$), suggesting that the PRC population specifically tuned to support both coherence and dynamics of neural representations between these epochs. Such a strong correlation was absent in the transition of the population response between the baseline epoch and the cue or reward epochs ($r = 0.021$, $P = 0.501$). Importantly, the correlation depended on the temporal response patterns in the individual neurons ($r = 0.088$, $P = 0.005$ for shuffled responses), suggesting that coherent single-neuron responses were critical to efficiently enhance the coherence and dynamics of the population encodings. Taken together, these findings indicated that the PRC population reconciles coherent representations of choice directions with dynamic representations for different epochs via temporally flexible but structured neural responses (that is, inverted selectivity between epochs).

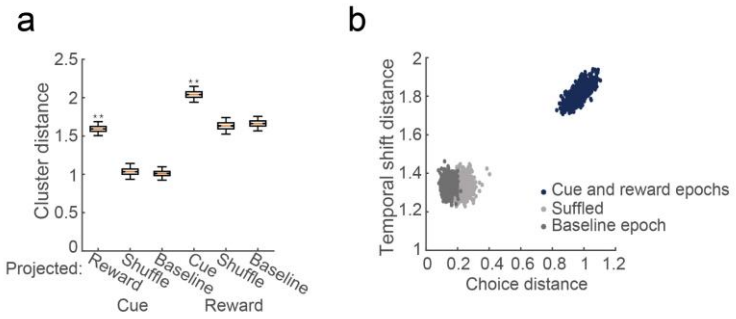

Figure 20 | Flexible response changes for the different epochs and sustained choice-direction encodings.

(**a**) Temporal shifts in the representational geometry. The same shuffled data as in Fig. 18b was shown here. The baseline-epoch responses were considered to be a chance level. (**b**) Relationship between temporal coherence and dynamics of the PRC population responses. Each single point corresponds to the population response in a subset of trials. The discriminability by the cue-epoch and reward-epoch responses is shown as blue points. The same for the baseline-epoch responses and shuffled responses are shown as deep gray and light gray points, respectively. In box plots: orange line, median; box limits, 25th and 75th quartiles; notch limits, (1.57 × interquartile range)/$\sqrt{n}$; whiskers, 95th percentile range (two-sided) of the distribution. Asterisks indicate statistical significance based on estimated P values ($P < 0.05$; Methods).

Chapter 4. Discussion

I investigated how coherent single-neuron representations across different epochs can be reconciled with the temporal dynamics of a population structure. Individual neurons in the PRC modulated their firings according to the different choice directions in each trial, and many neurons inverted such selectivity between the cue and reward epochs. Despite the structured temporal response patterns, I found a dynamic reorganization of the population encoding structure between the different epochs (that is, neural subspaces supported by different coordination patterns across neurons). Yet, I also found shared neural dimensions between the cue and reward epochs, where the choice-direction information was consistently represented throughout the epochs. Those dimensions depended on the coherent temporal patterns of the single-neuron responses. These findings indicated that the temporally structured single-neuron responses worked as a dynamic population structure, supporting coherent representations throughout multiple epochs of a given task (**Fig.** 21).

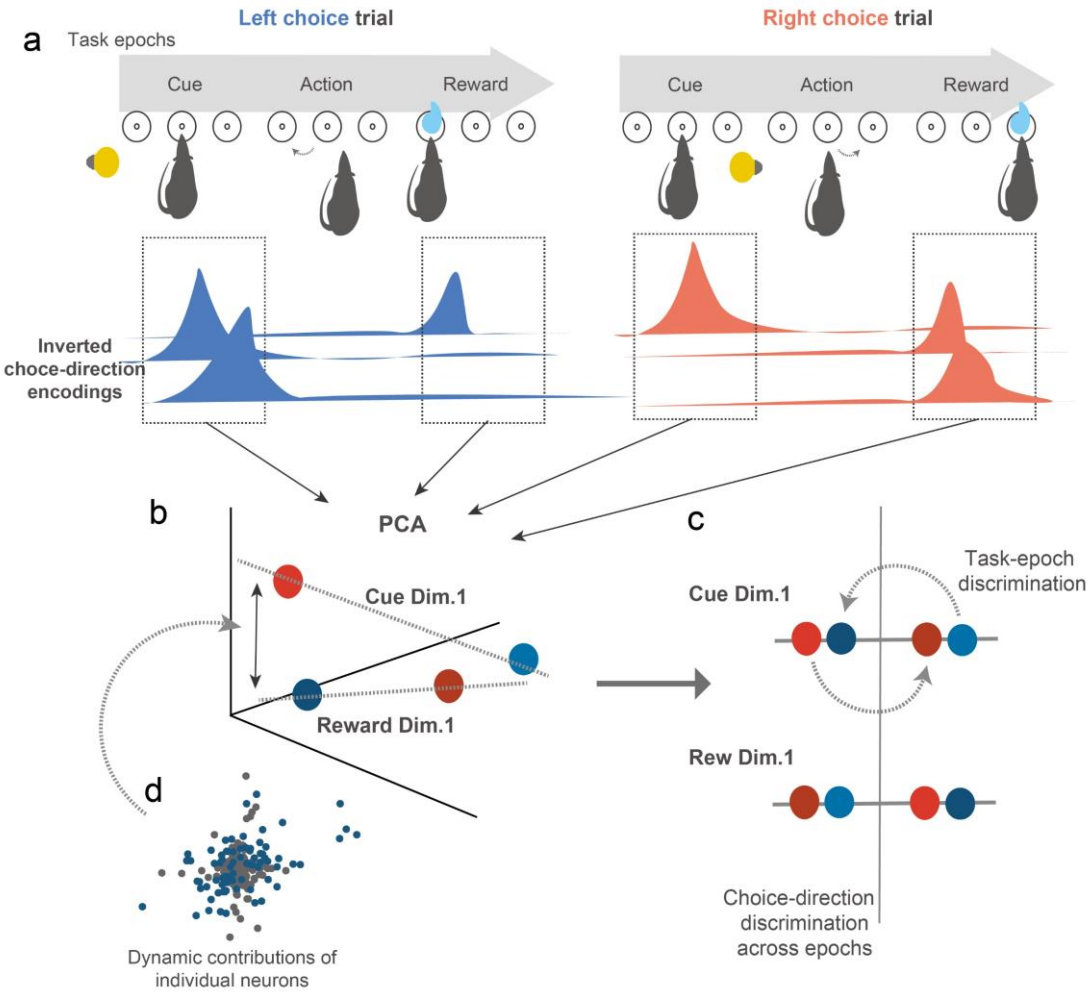

Figure 21 | A summary of the findings in the present study.

(**a**) The individual neurons in the PRC showed the inverted choice-direction encodings (blue, left choice; red, right choice) between the cue and reward epochs, suggesting a form of temporally coherent neural representation in the PRC. (**b**) Our population-level analysis showed that the first dimensions of the cue and reward epochs captured the difference of choice-directions (light colors, cue-epoch responses; dark colors, reward-epoch responses). (**c**) These first dimensions consistently discriminated the choice directions across the epochs. Also, the difference of task epochs was discriminated on these dimensions. (d) These shared dimensions were supported by the individual neurons that changed their contributions to the population-level encodings between the epochs in a heterogeneous manner. This suggests unique computational roles of individual neurons that hold temporally coherent representations across different task-epochs.

4.1. “Choice-direction” encodings in the PRC

4.1.1. Confounding variables underlying choice-related encodings in higher-order cortical areas

It is recently suggested that choice-related encodings observed in higher-order cortical areas are not necessarily abstract signals but rather parsimoniously explained by combinations of fundamental behavioral and contextual variables such as a specific spatial position and head angle (Krumin et al., 2018). Additionally, a recent study in rats revealed that neurons in the lateral entorhinal cortex, which is a down-stream region of the PRC, are sensitive to subtle changes of egocentric view (Wang et al., 2018). In contrast to these results, I revealed that the choice directions were a better predictor for the individual PRC neural responses than other major variables previously noted, namely, body posture, non-orienting movements, and spatial view (**Fig. 11**). Although those individual factors could influence the PRC responses, I found that they were not unique to evoke the PRC responses. Thus, I conclude that the choice-direction encodings in the PRC are an abstract signal integrating various computations related to the choice at a given epoch.

4.1.2. Different computations underlying choice-direction encodings of the PRC neurons

How does the nature of the choice-direction encodings differ between the cue and reward epochs? In the cue epoch, I did not find a significant difference between the choice-direction encodings in the correct and erroneous trials (**Fig. 13e–f**). Given that those neural responses are better explained by the choice directions than by head angles (**Fig. 11**), the cue-epoch responses might reflect internal signals such as a reward expectation, motor preparation, or decision (Eradath et al., 2015; Ohyama et al., 2012; Clark et al., 2012; Mogami & Tanaka, 2006; Liu et al., 2000). Contrary, in the reward epoch, the choice-direction encodings significantly decreased in the erroneous trials (**Fig. 13e–f**), conveying reward signals in conjunction with choice directions (**Fig. 11d–e**). Those distinct choice-related representations were not expected by previous studies, most of which highlight perceptual and mnemonic representations in the PRC (Ahn et al., 2019; Nelson et al., 2016; Ahn & Lee, 2015; Ho et al., 2015; Bartko et al., 2007; Naya et al., 2003a; 2003b; Naya et al., 1996; Sakai & Miyashita, 1991). However, a recent study suggests that the PRC is also involved in value-based decision making (Kreher et al., 2019).

In light of widespread anatomical connections of the PRC (Tomas Pereira et al., 2016; Furtak et al., 2007; Burwell, 2001), it is possible that this region flexibly carries diverse information besides perceptual and mnemonic signals depending on neural computation required for the task (Bos et al., 2017).

4.2. Coherent choice-direction encodings between the cue and reward epochs and their functional implication

The above results emphasize different neural computations reflected in the choice-direction selectivity in each of the cue and reward epochs. In spite of the explicit difference, the PRC neurons often showed choice-direction encodings in both epochs, suggesting that they support associative representations of choice and its outcome. This agrees with a traditional view, which holds that the PRC supports associative memory (Ahn & Lee, 2015; Naya et al., 2003a; 2003b; Naya et al., 1996; Sakai & Miyashita, 1991). Several studies showed that temporally sustained responses were prevalent in the PRC (Naya et al., 2017; Eradath et al., 2015; Naya & Suzuki, 2011; Sakai & Miyashita, 1991). Such sustained responses were found in studies focusing on neural responses during cue and memory epochs and were considered to serve as stable representations of targeted information across multiple epochs, which enable typical functions of the PRC including recognition memory (Meunier et al., 1993). The finding of the inverted response patterns was not predicted by those previous studies but suggested its advantage in supporting both temporal coherence and flexibility of neural

representations. Moreover, an important finding in this study is that the discriminability of the choice directions and task epochs was highly correlated (**Fig. 20b**). This encoding strategy might provide a synthesized view upon the role of the PRC in forming integrated representations of information with shared features and in discriminating between them. Although those functions have been generally tested in visual perception, findings in this study emphasize its multimodal nature (Kreher et al., 2019).

4.3. Neurons with coherent choice-direction encodings worked as a dynamic population

It is worth mentioning that the values of the neural weights of the individual neurons varied between the cue and reward epochs. In spite of the heterogeneity in individual neurons, at the population-level, the neural weights were moderately correlated between the epochs, resulting in the coherent choice-direction representations (**Fig. 19**). Heterogeneous response properties across individual neurons are often observed in high-order cortical areas (Hwang et al., 2017; Spaak et al., 2017; Meister et al., 2013; Harvey et al., 2012; Erlich et al., 2011; Jun et al., 2010) and are considered to increase the number of dimensions can be represented by a neural population (Parthasarathy et al., 2017; Barak et al., 2013; Miller & Fusi, 2013; Rigotti et al., 2013). In some cases, neurons exhibit a high degree of heterogeneity, in which multiple variables were randomly mixed at the individual neurons (Raposo et al., 2014; Mante et al., 2013). This 'random mixed selectivity' provides orthogonal neural subspaces where different neural computations that can be performed independently. In light of these ideas, the moderately correlated neural subspaces between the cue and reward epochs exhibit

balanced coherence and dynamics of the neural representations in the PRC, which might enable integrated processing of a targeted variable and contextual information and unique contribution to episodic memory as reported by previous studies (Naya et al., 2017; Naya & Suzuki, 2011).

4.4. Outlook

Although I did not detect any explicit clusters based on the response property of the PRC neurons (**Fig. 19a**), it is possible that they can be categorized into subpopulations based on different projection or cell types (Hirokawa et al., 2019). According to this idea, the heterogeneity among the PRC neurons possibly reflects different information routing to downstream regions such as the lateral entorhinal cortex and the hippocampus. For instance, it is possible that the neurons strongly inverted choice-direction encoding between the cue and reward epochs can contribute to pattern separation served by the CA3 region (Leutgeb et al., 2007). Also, the neurons carried more choice-direction information in the reward epoch might contribute to integrated reward representations in the CA1 region, in which individual neurons convey multiple reward positions (Gauthier et al., 2018). Given the potentially various anatomical properties of neurons, future studies should combine analytical and rigorous anatomical approaches to a gain deeper understanding for how a given population contributes to a larger process carried across multiple brain regions (Hirokawa et al., 2019).

Chapter 5. References

Ahn, J.R. & Lee, I. Neural correlates of both perception and memory for objects in the rodent perirhinal cortex. *Cereb. Cortex.* **27**, 3856–3868 (2017).

Ahn, J.R. & Lee, I. Neural correlates of object-associated choice behavior in the perirhinal cortex of rats. *J. Neurosci.* **35**, 1692–1705 (2015).

Ahn, J.R., Lee, H.W. & Lee, I. Rhythmic pruning of perceptual noise for object representation in the hippocampus and perirhinal cortex in rats. *Cell Rep.* **26**, 2362–2376 (2019).

Akhlaghpour, H. et al. Dissociated sequential activity and stimulus encoding in the dorsomedial striatum during spatial working memory. *Elife* **5**, e19507 (2016).

Barak, O., Rigotti, M. & Fusi, S. The sparseness of mixed selectivity neurons controls the generalization-discrimination trade-off. *J. Neurosci.* **33**, 3844–3856 (2013).

Bartko, S. J., Winters, B. D., Cowell, R. A., Saksida, L. M. & Bussey, T. J. Perceptual functions of perirhinal cortex in rats: zero-delay object recognition and simultaneous oddity discriminations. *J Neurosci* **27**, 2548–2559 (2007).

Bos, J.J. et al. Perirhinal firing patterns are sustained across large spatial segments of the task environment. *Nat. Commun.* **8**, 15602 (2017).

Bruce, C., Desimone, R. & Gross, C. G. Visual properties of neurons in a polysensory area in superior temporal sulcus of the macaque. *J. Neurophysiol.* **46**, 369–384 (1981).

Burwell, R. D. Borders and cytoarchitecture of the perirhinal and postrhinal cortices in the rat. *J. Comp. Neurol.* **437**, 17–41 (2001).

Cavanagh, S. E., Towers, J. P., Wallis, J. D., Hunt, L. T. & Kennerley, S. W. Reconciling persistent and dynamic hypotheses of working memory coding in prefrontal cortex. *Nat. Commun.* **9**, 1–16 (2018).

Clark, A. M., Bouret, S., Young, A. M. & Richmond B. J. Intersection of reward and memory in monkey rhinal cortex. *J. Neurosci.* **32**, 6869–6877 (2012).

Elsayed, G. F., Lara, A. H., Kaufman, M. T., Churchland, M. M. & Cunningham, J. P. Reorganization between preparatory and movement population responses in motor cortex. *Nat. Commun.* **7**, 13239 (2016).

Eradath, M. K., Mogami, T., Wang, G. & Tanaka, K. Time context of cue-outcome associations represented by neurons in perirhinal cortex. *J. Neurosci.* **35**, 4350–4365 (2015).

Erlich, J. C., Bialek, M. & Brody, C. D. A cortical substrate for memory-guided orienting in the rat. *Neuron* **72**, 330–343 (2011).

Fujisawa, S., Amarasingham, A., Harrison, M. T. & Buzsáki, G. Behavior-dependent short-term assembly dynamics in the medial prefrontal cortex. *Nat. Neurosci.* **11**, 823 (2008).

Furtak, S. C., Wei, S.M., Agster, K. L. & Burwell, R. D. Functional neuroanatomy of the parahippocampal region in the rat: the perirhinal and postrhinal cortices. *Hippocampus* **17**, 709–722 (2007).

Furuyashiki, T., Holland, P. C. & Gallagher, M. Rat orbitofrontal cortex separately encodes response and outcome information during performance of goal-directed behavior. *J. Neurosci.* **28**, 5127–5138 (2008).

Gardner, M. P. H. & Fontanini, A. Encoding and tracking of outcome-specific expectancy in the gustatory cortex of alert rats. *J. Neurosci.* **34**, 13000–13017 (2014).

Gauthier, J. L. & Tank, D. W. A dedicated population for reward coding in the hippocampus. *Neuron* **99**, 179–193.e7 (2018).

Green D. M. & Swets J. A. *Signal detection theory and psychophysics*. (Wiley, New York, 1966)

Guo, Z. V. et al. Maintenance of persistent activity in a frontal thalamocortical loop. *Nature*. **545**, 181–186 (2017).

Handa, T., Takekawa, T., Harukuni, R., Isomura, Y. & Fukai, T. Medial frontal circuit dynamics represents probabilistic choices for unfamiliar sensory experience. *Cereb. Cortex* **27**, 3818–3831 (2017).

Harvey, C. D., Coen, P. & Tank, D. W. Choice-specific sequences in parietal cortex during a virtual-navigation decision task. *Nature* **484**, 62–68 (2012).

Hirokawa, J. et al. Multisensory information facilitates reaction speed by enlarging activity difference between superior colliculus hemispheres in rats. *PLoS One* **6**, (2011).

Hirokawa, J., Vaughan, A., Masset, P., Ott, T. & Kepecs, A. Frontal cortex neuron types categorically encode single decision variables. *Nature* **576**, 446–451 (2019).

Ho, J. W. et al. Bidirectional modulation of recognition memory. *J. Neurosci.* **35**, 13323–13335 (2015).

Hosokawa, T., Kato, K., Inoue, M. & Mikami, A. Correspondence of cue activity to reward activity in the macaque orbitofrontal cortex. *Neurosci. Lett.* **389**, 146–151 (2005).

Hubel, D. H. & Wiesel, T. N. Receptive fields of single neurones in the cat's striate cortex. *J. Physiol.* **148**, 574–591 (1959).

Hwang, E. J., Dahlen, J. E., Mukundan, M. & Komiyama, T. History-based action selection bias in posterior parietal cortex. *Nat. Commun.* **8**, 1242 (2017).

Jun, J. K. et al. Heterogenous population coding of a short-term memory and decision task. *J. Neurosci.* **30**, 916–929 (2010).

Kennerley, S. W. & Wallis, J. D. Evaluating choices by single neurons in the frontal lobe: outcome value encoded across multiple decision variables. *Eur. J. Neurosci.* **29**, 2061–2073 (2009).

Kreher, M.A. et al. The perirhinal cortex supports spatial intertemporal choice stability. *Neurobiol. Learn. Mem.* **162**, 36–46 (2019).

Krumin, M., Lee, J. J., Harris, K. D., & Carandini, M. Decision and navigation in mouse parietal cortex. *eLife* **7**, e42583 (2018).

Lara, A. H., Cunningham, J. P. & Churchland, M. M. Different population dynamics in the supplementary motor area and motor cortex during reaching. *Nat. Commun.* **9**, (2018).

Leutgeb, J. K., Leutgeb, S., Moser, M. B. & Moser, E. I. Pattern separation in the dentate gyrus and CA3 of the hippocampus. *Science* **315**, 961–966 (2007).

Liu, Z., Murray, E. A. & Richmond, B. J. Learning motivational significance of visual

cues for reward schedules requires rhinal cortex. *Nat. Neurosci.* **3**, 1307–1315 (2000).

Mante, V., Sussillo, D., Shenoy, K. V & Newsome, W. T. Context-dependent computation by recurrent dynamics in prefrontal cortex. *Nature*. **503**, 78–84 (2013).

Meister, M. L., Hennig, J. A. & Huk, A. C. Signal multiplexing and single-neuron computations in lateral intraparietal area during decision-making. *J. Neurosci.* **33**, 2254–2267 (2013).

Mendoza-Halliday, D. & Martinez-Trujillo, J. C. Neuronal population coding of perceived and memorized visual features in the lateral prefrontal cortex. *Nat. Commun.* **8**, 15471 (2017).

Meunier, M., Bachevalier, J., Mishkin, M. & Murray, E. A. Effects on visual recognition of combined and separate ablations of the entorhinal and perirhinal cortex in rhesus monkeys. *J. Neurosci.* **13**, 5418–5432 (1993).

Meyer, A.F., Poort, J., O'Keefe, J., Sahani, M. & Linden, J.F. A Head-mounted camera system integrates detailed behavioral monitoring with multichannel electrophysiology in freely moving mice. *Neuron* **100**, 46–60 (2018).

Miller, E. K. & Fusi, S. Limber neurons for a nimble mind. *Neuron* **78**, 211–213 (2013)

Mogami, T. & Tanaka, K. Reward association affects neuronal responses to visual stimuli

in macaque TE and perirhinal cortices. *J. Neurosci.* **26**, 6761–6770 (2006).

Morcos, A. & Harvey, C. History-dependent variability in population dynamics during evidence accumulation in cortex. *Nat Neurosci* **19,** 1672–1681 (2016).

Murray, J. D. et al. Stable population coding for working memory coexists with heterogeneous neural dynamics in prefrontal cortex. *Proc. Natl Acad. Sci.* USA **114**, 394–399 (2017).

Musall, S., Kaufman, M.T., Juavinett, A.L., Gluf, S. & Churchland, A.K. Single-trial neural dynamics are dominated by richly varied movements. *Nat. Neurosci.* **22**, 1677–1686 (2019).

Naya, Y. & Suzuki, W. A. Integrating what and when across the primate medial temporal lobe. *Science*. **333**, 773–776 (2011).

Naya, Y., Chen, H., Yang, C. & Suzuki, W. A. Contributions of primate prefrontal cortex and medial temporal lobe to temporal-order memory. *Proc. Natl. Acad. Sci. U. S. A.* **114**, 13555–13560 (2017).

Naya, Y., Sakai, K. & Miyashita, Y. Activity of primate inferotemporal neurons related to a sought target in pair-association task. *Proc. Natl. Acad. Sci. U. S. A.* **93**, 2664–2669 (1996).

Naya, Y., Yoshida, M. & Miyashita, Y. Forward processing of long-term associative memory in monkey inferotemporal cortex. *J. Neurosci.* **23**, 2861–2871 (2003a).

Naya, Y., Yoshida, M., Takeda, M., Fujimichi, R. & Miyashita, Y. Delay-period activities in two subdivisions of monkey inferotemporal cortex during pair association memory task. *Eur. J. Neurosci.* **18**, 2915–2918 (2003b).

Nelson, A. J., Olarte-Sánchez, C. M., Amin, E. & Aggleton, J.P. Perirhinal cortex lesions that impair object recognition memory spare landmark discriminations. *Behav. Brain Res.* **313**, 255–259 (2016).

Ohyama, K., Sugase-Miyamoto, Y., Matsumoto, N., Shidara, M. & Sato, C. Stimulus-related activity during conditional associations in monkey perirhinal cortex neurons depends on upcoming reward outcome. *J. Neurosci.* **32**, 17407–17419 (2012).

Parthasarathy, A. et al. Mixed selectivity morphs population codes in prefrontal cortex. *Nat. Neurosci.* **20**, 1770–1779 (2017).

Paxinos, G. & Watson, C. *The rat brain in stereotaxic coordinates*, *Sixth Edition* (Elsevier, Amsterdam, 2007)

Raposo, D., Kaufman, M. T. & Churchland, A. K. A category-free neural population supports evolving demands during decision-making. *Nat. Neurosci.* **17**, 1784–1792 (2014).

Rigotti, M. et al. The importance of mixed selectivity in complex cognitive tasks. *Nature* **497**, 585–590 (2013).

Sakai, K. & Miyashita, Y. Neural organization for the long-term memory of paired associates. *Nature*. **354**, 152–155 (1991).

Sakurai, Y. Cells in the rat auditory system have sensory-delay correlates during the performance of an auditory working memory task. *Behav. Neurosci.* **104**, 856–868 (1990a).

Sakurai, Y. Hippocampal cells have behavioral correlates during the performance of an auditory working memory task in the rat. *Behav. Neurosci.* **104**, 253–263 (1990b).

Sakurai,Y. et al. Multipotentiality of the brain to be revisited repeatedly. *The Physics of the Mind and Brain Disorders*: pp.513–525. (Springer, Cham, 2017)

Sanders, J. I. & Kepecs, A. A low-cost programmable pulse generator for physiology and behavior. *Front. Neuroeng.* **7**, 1–8 (2014).

Shiotani, K. et al. Tuning of ventral tenia tecta neurons of the olfactory cortex to distinct scenes of feeding behavior. Preprint at https://www.biorxiv.org/content/10.1101/455089v1 (2018).

Shuler, M. G. & Bear, M. F. Reward timing in the primary visual cortex. *Science* **311**,

1606–1609 (2006).

Siniscalchi, M. J., Wang, H. & Kwan, A. C. Enhanced population coding for rewarded choices in the medial frontal cortex of the mouse. *Cereb. Cortex*, **29**, 4090–4106 (2019).

Spaak, E., Watanabe, K., Funahashi, S. & Stokes, M. G. Stable and Dynamic Coding for Working Memory in Primate Prefrontal Cortex. *J. Neurosci.* **37**, 6503–6516 (2017).

Steinmetz, N. A., Zatka-Haas, P., Carandini, M. & Harris, K. D. Distributed coding of choice, action and engagement across the mouse brain. *Nature* **576,** 266–273 (2019).

Stokes, M. G. et al. Dynamic coding for cognitive control in prefrontal cortex. *Neuron.* **78**, 364–375 (2013).

Tomas Pereira, I. et al. Subcortical connections of the perirhinal, postrhinal, and entorhinal cortices of the rat. I. afferents. *Hippocampus* **26**, 1189–1212 (2016).

Wang, C. et al. Egocentric coding of external items in the lateral entorhinal cortex. *Science* **362**, 945–949 (2018).

Yoshizawa, T., Ito, M. & Doya, K. Reward-predictive neural activities in striatal striosome compartments. *eNeuro*, **5**, e0367-17. (2018).